AD-A112 821 FLORIDA UNIV GAINESVILLE DEPT OF ENGINEERING SCIENCES F/G 21/1
A FINITE ELEMENT-DIFFERENTIAL METHOD FOR INCOMPRESSIBLE TURBULE--ETC(U)
FEB 82 T CHANG, C HSU F33615-81-K-3210
UNCLASSIFIED AFWAL-TR-81-3174 NL

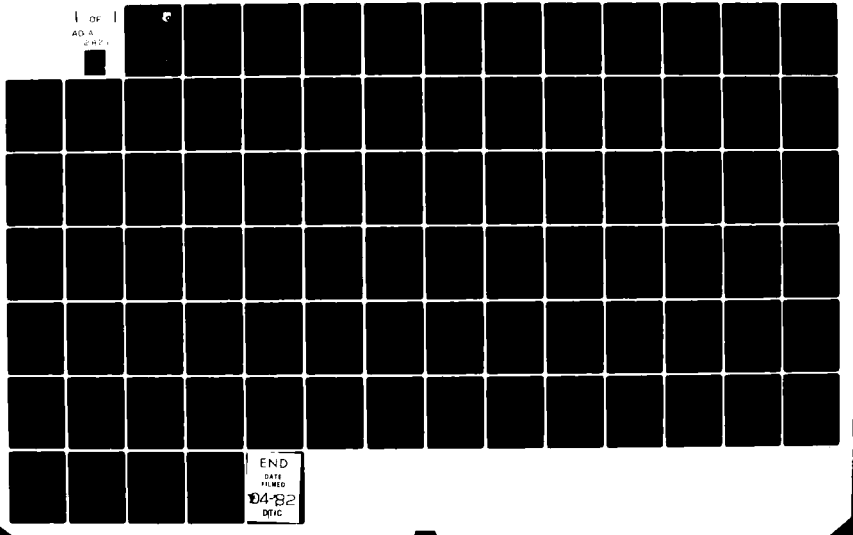

END
DATE FILMED
04-82
DTIC

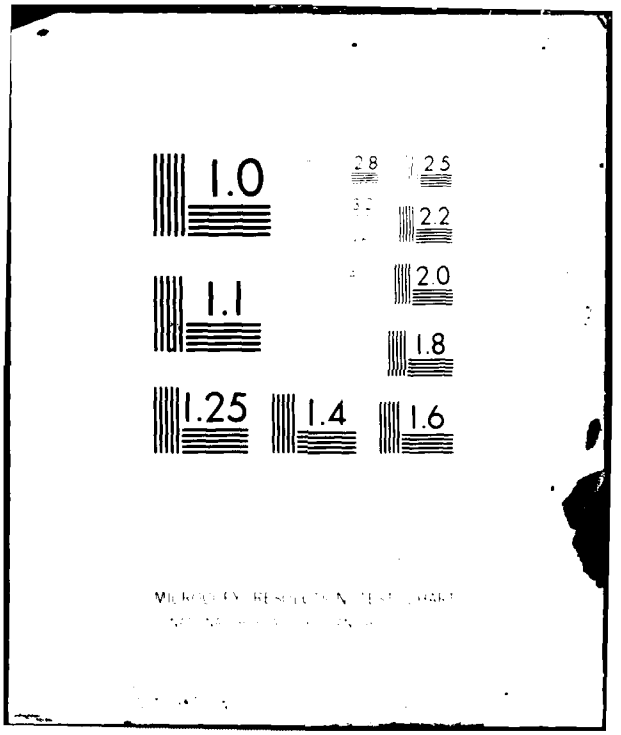
1.0
2.8
2.5
2.2
1.1
2.0
1.8
1.25
1.4
1.6

AFWAL-TR-81-3174

A FINITE ELEMENT-DIFFERENTIAL METHOD FOR INCOMPRESSIBLE TURBULENT BOUNDARY-LAYER FLOWS

TYNE-HSIEN CHANG

CHEN-CHI HSU

Department of Engineering Sciences
University of Florida
Gainesville, Florida 32611

February 1982
Report for Period Jan 1980 - Aug 1981

FLIGHT DYNAMICS LABORATORY
AIR FORCE WRIGHT AERONAUTICAL LABORATORIES
AIR FORCE SYSTEMS COMMAND
WRIGHT-PATTERSON AIR FORCE BASE, OHIO 45433

NOTICE

When Government drawings, specifications, or other data are used for any purpose other than in connection with a definitely related Government procurement operation, the United States Government thereby incurs no responsibility nor any obligation whatsoever; and the fact that the government may have formulated, furnished, or in any way supplied the said drawings, specifications, or other data, is not to be regarded by implication or otherwise as in any manner licensing the holder or any other person or corporation, or conveying any rights or permission to manufacture use, or sell any patented invention that may in any way be related thereto.

This report has been reviewed by the Office of Public Affairs (ASD/PA) and is releasable to the National Technical Information Service (NTIS). At NTIS, it will be available to the general public, including foreign nations.

This technical report has been reviewed and is approved for publication.

Charles L. Keller

CHARLES L. KELLER
Mathematician
Aeroelastic Group
Analysis & Optimization Branch

Fred A. Picchioni

FREDERICK A. PICCHIONI, LtCol, USAF
Analysis & Optimization Branch
Structures & Dynamics Division

FOR THE COMMANDER

RALPH L. KUSTER, Jr., Col, USAF
Chief, Structures & Dynamics Division

"If your address has changed, if you wish to be removed from our mailing list, or if the addressee is no longer employed by your organization please notify AFWAL/FIBRC, *W-PAFB, OH 45433 to help us maintain a current mailing list".*

Copies of this report should not be returned unless return is required by security considerations, contractual obligations, or notice on a specific document.

AIR FORCE/56780/5 March 1982 — 100

Unclassified

SECURITY CLASSIFICATION OF THIS PAGE (When Data Entered)

REPORT DOCUMENTATION PAGE	READ INSTRUCTIONS BEFORE COMPLETING FORM
1. REPORT NUMBER: AFWAL-TR-81-3174	2. GOVT ACCESSION NO. AD-A112 421
3. RECIPIENT'S CATALOG NUMBER	
4. TITLE (and Subtitle): A FINITE ELEMENT-DIFFERENTIAL METHOD FOR INCOMPRESSIBLE TURBULENT BOUNDARY LAYER FLOWS	5. TYPE OF REPORT & PERIOD COVERED: INTERIM REPORT Jan 1980 - Aug 1981
	6. PERFORMING ORG. REPORT NUMBER: THESIS
7. AUTHOR(s): Tyne-Hsien Chang Chen-Chi Hsu	8. CONTRACT OR GRANT NUMBER(s): F33615-81-k-3210
9. PERFORMING ORGANIZATION NAME AND ADDRESS: Department of Engineering Sciences University of Florida Gainesville, Florida 32611	10. PROGRAM ELEMENT, PROJECT, TASK AREA & WORK UNIT NUMBERS: DOD Element 61102F 2304N115
11. CONTROLLING OFFICE NAME AND ADDRESS: FLIGHT DYNAMICS LABORATORY (AFWAL/FIBRC) AIR FORCE WRIGHT AERONAUTICAL LABORATORIES (AFSC) Wright-Patterson AFB, OH 45433	12. REPORT DATE: February 1982 13. NUMBER OF PAGES: 79
14. MONITORING AGENCY NAME & ADDRESS (if different from Controlling Office)	15. SECURITY CLASS. (of this report): UNCLASSIFIED 15a. DECLASSIFICATION DOWNGRADING SCHEDULE

16. DISTRIBUTION STATEMENT (of this Report)

Approved for public release; distribution unlimited.

17. DISTRIBUTION STATEMENT (of the abstract entered in Block 20, if different from Report)

18. SUPPLEMENTARY NOTES

19. KEY WORDS (Continue on reverse side if necessary and identify by block number)

Incompressible turbulent boundary layer; finite element-differential method; two-layer eddy viscosity model; classical cubic splines; stiff equations; Gear's method.

20. ABSTRACT (Continue on reverse side if necessary and identify by block number)

The applicability as well as the accuracy and efficiency of a finite element-differential method, which had been shown to be very effective method for laminar flows, is investigated in detail for more complex steady two-dimensional incompressible turbulent boundary alyer flow problems. The closure model chosen for the turbulent flows is a two-layer eddy viscosity model. A number of important transformations have been carried out for the system of governing equations before the application of the proposed solution method.

DD FORM 1 JAN 73 1473

Unclassified

SECURITY CLASSIFICATION OF THIS PAGE (When Data Entered)

In the method of solution, the transformed partial differential equation is first reduced to a system of first order nonlinear ordinary differential equations by a subdomain collocation method, in which the unknown function at a streamwise station is represented by a classical spline function. The resulting initial value problem is then integrated numerically by the modified Hamming's predictor-corrector method as well as by Gear's method for stiff equations.

The numerical experiments have been conducted on the flat plate problem which consists of the laminar, transitional, and turbulent flow regions covering the range of local Reynolds numbers from 8×10^3 to 1×10^8. The study shows that the method of solution can be very efficient and provides highly accurate results for the turbulent flow problem. In fact the computed skin-friction coefficient distribution over the range of the Reynolds numbers considered agrees almost perfectly with the measured data. Moreover, the results of numerical experiments have provided some valuable information on the flow characteristics relevant to numerical approximations.

PREFACE

The work described in this Interim Technical Report was performed by Mr. Tyne-Hsien Chang under the supervision of the principal investigator Dr. Chen-Chi Hsu. This effort was started under grant AFOSR-80-0033 and completed under Contract No. F33615-81-K-3210 Development of Finite Element Differential Methods for External Flow Problems at High Reynolds Number to the University of Florida, Gainesville for the Applied Mathematics Group, Analysis and Optimization Branch, Structures and Dynamics Division, Flight Dynamics Laboratory, AFWAL under Project 2304 Research in Applied Mathematics, Task 2304N1 Computational Aspects of Fluid and Structural Mechanics and Program Element 61102F. The investigation was conducted during the period January 1980 through August 1981. This effort has been submitted as Mr. Chang's PhD dissertation to the Graduate Council of the University of Florida in partial fulfillment of the requirements for the degree of Doctor of Philosophy. Dr. Charles L. Keller, AFWAL/FIBRC, Wright-Patterson AFB, OH 45433, was the program manager.

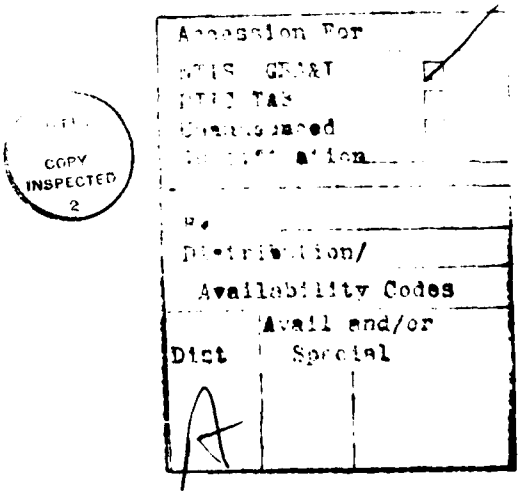

TABLE OF CONTENTS

LIST OF ILLUSTRATIONS

SECTION I
INTRODUCTION

In recent years there has been considerable research effort in the field of computational turbulent boundary layer flows because of the need for more accurate solutions to flow problems that arise in engineering applications. The turbulent boundary-layer flows are generally more complex than laminar boundary-layer flows in the sense that these flow problems do have their own distinct and important characteristics which may require special attention in the application of solution techniques. For instance, the growth of turbulent boundary-layer thickness occurs at a much faster but unknown rate, and the very thin viscous sublayer in the vicinity of the wall has an extremely large velocity gradient; consequently, special measures are needed in the discretization of the flow region. In general, large numbers of grid points with relatively small grid sizes must be specified near the wall in order to obtain an accurate solution.

The governing boundary layer equations for incompressible turbulent flows contain a term, called the Reynolds stress, which involves the time mean of the product of two fluctuating velocities. The Reynolds stress has been modeled by means of the mean velocity, of the turbulent energy, of the product of turbulent energy with a length scale, and of the Reynolds stress itself as the dependent variables of the differential equations; consequently the closure models for turbulent boundary-layer flows can be classified as zero equation, one-equation, two-equation,

and stress-equation models. The zero-equation models are easier to formulate and calibrate and therefore have been used extensively to provide predictions for engineering problems. Other closure models are more complex and their use for practical problems is rather limited at present. Reynolds [1] provided an overview of the closure models and concluded that the zero-equation model has been applied to a variety of turbulent flows and works quite well for most turbulent boundary layer flows considered at Stanford conference, a special conference was held at Stanford Universtiy in 1968 to compare the viability of prediction methods based on various closure models for the partial differential equations describing turbulent boundary layer flows. In addition, the Stanford conference provided a direct check on the accuracy of the various prediction methods. A total of nine methods of solving governing partial differential equations with a closure model competed. The results of the conference indicated that the prediction methods of Mellor and Herring [2], Cebeci and Smith [3], and Ng, Patankar and Spalding [4] can provide acceptably accurate solution for the flow problems considered. The solution of Mellor and Herring with the effective eddy viscosity model is obtained completely across the boundary layer. They used the Hartree-Womersley semi-discrete method for solving the governing equations, where the ordinary differential equations are solved across the layer using the Runge-Kutta integration procedure. Ng, Patankar and Spalding selected a mixing length model and used a Crank-Nicolson type of finite-difference scheme, which is not applied to the wall. Instead, a wall function is introduced that gives the flow quantities at the wall. Cebeci and Smith used an implicit finite-difference scheme to obtain the solution across the

complete boundary layer with the eddy viscosity model. Several hundred grid points across the boundary layer had been used by the above mentioned finite difference methods for accurate solution.

Recently, the two-layer eddy viscosity closure model has been extensively used in solving practical turbulent flow problems. This model consists of inner and outer regions, and the distributions of eddy viscosity are described by two separate empirical expressions in the two regions (e.g. Cebeci and Smith, [5]). The expression for eddy viscosity in the inner region is based on mixing length theory, and a modified expression for the mixing length is used to account for the viscous sublayer close to the wall. The expression for eddy viscosity in the outer region is based on a constant eddy viscosity modified by a transverse intermittency factor. This model has been accepted as the standard form of the zero-equation model and used by many researchers to develop computational methods for turbulent flow problems.

Keller and Cebeci [6] applied a Levy-Lees Transformation to the governing equations and then used the well known box scheme with Richardson extrapolation to obtain the solution for turbulent flow over a flat plate. The flow region considered is from the local Reynolds number $Re_x = 0.83 \times 10^3$ to $Re_x = 1.88 \times 10^6$ with constant boundary layer thickness. The numerical solutions, using Keller's box scheme based on 11, 21, and 31 grid points across the boundary layer with the designed variable-grid system, were obtained at 17 different stations in the streamwise direction. The results of the 31-grid scheme are acceptably accurate but the results of the other two schemes are not acceptable; however, the accuracy of solutions can be improved by the Richardson extrapolation. These results show that Keller's box scheme

with Richardson extrapolation can be very simple and accurate for turbulent flows.

Blottner [7] pointed out that Keller's box scheme requires the solution of block-tridiagonal equations and can be very time consuming when extended to compressible boundary layer flows. Consequently, he proposed a Crank-Nicolson type of difference scheme with a variable grid and solved the same flat plate problem. The results obtained indicated that the Crank-Nicolson type scheme is easier to formulate and can give the same accuracy as Keller's box scheme for the turbulent boundary layer flow. In addition, the number of grid points required for the Crank-Nicolson method is less than that of Keller's box scheme under the same accuracy requirement.

Recently Rubin and Khosla [8] have extended their higher-order collocation method to turbulent flows with some success. The higher-order collocation method derived from polynomial spline interpolation and Hermite collocation is used to overcome the stiffness problem caused by the extremely small grid size near the boundary. Again, they chose the flow over a flat plate as the testing example. The solutions were obtained for the range $5.45 \times 10^4 \leq Re_x \leq 2 \times 10^6$. For the Reynolds number considered here they only used 11 grid points across the boundary layer, with first element size $h_1 = 0.1432$, to provide 5-10% accuracy. With 21 points and $h_1 = 0.005$ the results are well within the experimental scatter. Indeed the method can also provide accurate results. It should be pointed out, however, that an iterative method can lead to erroneous solutions if the truncation error of the approximation is large. This fact is evident from the results of the numerical experiments given in Rubin and Khosla (1977).

More recently a finite element-differential method has been developed and tested successfully for two-dimensional laminar boundary layer flows (Hsu, [9] and Hsu and Liakopoulos, [10]). The application of the method is very simple and straightforward; however, one must carry out a number of transformations in the analysis first. In this method the transformed flow region is divided into a number of strips parallel to the boundary and the unknown functions at a given streamwise station are approximated by classical cubic splines. The transformed governing partial differential equations are then reduced to a system of first order nonlinear ordinary differential equations by a subdomain collocation method; consequently, the resulting initial value problem is solved by a numerical integration method. The stiff problem associated with the reduced equations may be pronounced if one used a great number of strips and very small element sizes near the wall. The numerical results obtained showed that the method is indeed very efficient and can provide highly accurate results for the entire flow region.

It seems that the finite element-differential method developed is a rather promising solution technique for more complex flow problems. The objective of this study is, therefore, to investigate the applicability as well as the accuracy and efficiency of the finite element-differential method to more complex two dimensional incompressible turbulent boundary-layer flows. The governing boundary layer equations with the two-layer eddy viscosity closure model have been transformed into the proper forms for applying the solution technique.

The applicability, accuracy and efficiency of the solution method for complex turbulent boundary layer flows have been investigated in detail upon the flat plate problem. The boundary layer flow considered

consists of the laminar, transitional, and turbulent regions which covers the range of local Reynolds numbers from $Re_x = 8.1 \times 10^3$ to $Re_x = 1.1 \times 10^8$. The results obtained have shown that the finite element-differential method can be very efficient and provide highly accurate solution for the turbulent boundary layer flow problems. Moreover, the result of numerical experiments has given valuable information on the flow characteristics relevant to numerical approximation.

CHAPTER II
GOVERNING BOUNDARY-LAYER EQUATIONS

For two-dimensional, steady, incompressible turbulent boundary layer flows, the governing equations are (e.g. White, [11])

$$\frac{\partial u}{\partial x} + \frac{\partial v}{\partial y} = 0 \ , \tag{2-1}$$

$$\rho\left(u \frac{\partial u}{\partial x} + v \frac{\partial u}{\partial y}\right) = \frac{\partial}{\partial y}\left(\mu \frac{\partial u}{\partial y} - \rho\overline{u'v'}\right) + \rho U \frac{dU}{dx} \ , \tag{2-2}$$

where

x = the coordinate along the boundary in the direction of flow,

y = the coordinate normal to the boundary,

u = mean velocity component in x direction,

v = mean velocity component in y direction,

u' = fluctuating velocity component in x direction,

v' = fluctuating velocity component in y direction,

U = velocity just outside the boundary layer,

μ = dynamic viscosity,

ρ = fluid density.

The associated boundary and initial conditions considered are

$$u(x, 0) = 0 \ , \ v(x, 0) = 0 \ , \ u(x, y \to \infty) \to U(x) \ , \tag{2-3}$$

$$u(0, y) = u_0(y) \ . \tag{2-4}$$

In equation (2-2) $-\rho\overline{u'v'}$ is called Reynolds stress which is caused by the action of turbulence. When the Reynolds stress is zero, equations

(2-1)-(2-4) are the governing equations for laminar boundary-layer flows. Equations (2-1)-(2-4) are not complete; a closure model to make the system closed is needed. The purpose of a closure model is to relate the Reynolds stress to other flow quantities and thereby obtain a closed system of equations.

There are several levels of closure models available (Reynolds, 1976). The zero-equation model, based on algebraic eddy viscosity formulation, has been tested for a wide range of turbulent boundary layer flows with considerable success. The one-equation model, in which a partial differential equation for the turbulence energy is solved in conjunction with the partial differential equations for the mean motion, finds use in practical applications on occasion. The two-equation model, obtained by adding an additional partial differential equation for the turbulence length scale to the one-equation model, has not been used extensively for engineering problems, although it is currently popular among researchers. The stress-equation model, which involves partial differential equations for all components of the turbulent stress tensor, is now under intensive development.

Due to its simple formulations and wide applications in various engineering problems, the two-layer eddy viscosity model is used in the present analysis. The development of this model is discussed in some detail in appendix A. According to the model, the kinematic eddy viscosity, ν_t, is defined by

$$\nu_t \equiv \frac{\overline{-u'v'}}{\frac{\partial u}{\partial y}} \quad . \tag{2-5}$$

The effective eddy viscosity is defined by

$$\nu_e = \nu_t + \nu \quad , \tag{2-6}$$

where ν is the kinematic laminar viscosity. Consequently, the distribution of the two-layer effective eddy viscosity across the boundary layer including the transitional and transverse intermittency factors can be written as (appendix A, equations (A-12) and (A-13))

$$(\nu_e)_i = \nu + \{0.4y[1 - \exp(\frac{-y}{A})]\}^2 |\frac{\partial u}{\partial y}| \gamma_t \quad , \tag{2-7}$$

$$(\nu_e)_0 = \nu + 0.0168\, U(x)\delta^* \gamma \gamma_t \quad , \tag{2-8}$$

where subscripts i and 0 represent the inner and outer regions, respectively. The damping constant A, transitional intermittency factor γ_t, transverse intermittency factor γ, and displacement boundary layer thickness δ^*, as discussed in appendix A, are

$$A = (26\frac{\nu}{U_\tau}) (1 - 11.8 \frac{\nu}{\rho U_\tau^3} \frac{dp}{dx})^{-\frac{1}{2}} \quad , \tag{2-9}$$

$$\gamma_t = 1 - \exp\left[\frac{-1}{1200} (\frac{U^3(x)}{\nu^2}) R_{x_{tr}}^{-1.34} (x - x_{tr}) \int_{x_{tr}}^{x} \frac{ds}{U(s)}\right] , \tag{2-10}$$

$$\gamma = [1 + 5.5\, (y/\delta)^6]^{-1}, \tag{2-11}$$

$$\delta^* = \int_0^\infty (1 - \frac{u}{U})dy \quad , \tag{2-12}$$

where x_{tr} is the location of the start of transition and δ is the boundary layer thickness. The friction velocity, u_τ, and the transition Reynolds number, $R_{x_{tr}}$, are defined by the following expressions, respectively,

$$u_\tau \equiv (\tau_w(x)/\rho)^{\frac{1}{2}} \quad , \tag{2-13}$$

$$R_{x_{tr}} \equiv \frac{U(x)X_{tr}}{\nu} \quad , \tag{2-14}$$

where $\tau_w(x)$ is shear stress at wall.

The matching point which separates the inner and outer regions must be determined from the continuity of the eddy viscosity, that is,

$$(\nu_e)_i = (\nu_e)_0 \quad . \tag{2-15}$$

Therefore, the complete set of the governing boundary layer equations for the flow problem considered is given by

$$\frac{\partial u}{\partial x} + \frac{\partial v}{\partial y} = 0 \quad , \tag{2-16}$$

$$u\frac{\partial u}{\partial x} + v\frac{\partial u}{\partial y} = \frac{\partial}{\partial y}\left(\nu_e \frac{\partial u}{\partial y}\right) + U\frac{dU}{dx} \quad , \tag{2-17}$$

$$\nu_e = \begin{cases} (\nu_e)_i \text{ given by equation (2-7)} \\ (\nu_e)_0 \text{ given by equation (2-8)} \quad , \end{cases} \tag{2-18}$$

$$u(x, 0) = 0 \quad , \quad v(x, 0) = 0 \quad , \quad u(x, y\to\infty) \to U(x) \quad , \tag{2-19}$$

$$u(0, y) = u_0(y) \quad . \tag{2-20}$$

The important physical quantity besides the velocity flow field is the wall shear stress distribution, $\tau_w(x)$, which is defined by

$$\tau_w(x) \equiv \left[\rho\nu_e \frac{\partial u}{\partial y}\right]_{y=0} \quad . \tag{2-21}$$

As usual the local skin-friction coefficient C_f is defined by

$$C_f \equiv \frac{\tau_w(x)}{\frac{1}{2}\rho U^2(x)} \quad . \tag{2-22}$$

CHAPTER III
TRANSFORMED BOUNDARY-LAYER EQUATIONS

In solving boundary layer flow problems governed by equations (2-16)-(2-20), it is often advantageous to carry out a number of coordinate transformations before application of a solution method. First, the governing equations can be made dimensionless by the following transformations:

$$x_1 = \frac{x}{L} \quad , \quad y_1 = \frac{y}{L} \quad , \tag{3-1}$$

$$u_1(x_1, y_1) = \frac{u(x, y)}{U_\infty} \quad , \quad v_1(x_1, y_1) = \frac{v(x, y)}{U_\infty} \quad , \quad U_1(x_1) = \frac{U(x)}{U_\infty} \quad ,$$

in which L and U_∞ are the characteristic length and velocity. The resulting non-dimensional equations are

$$\frac{\partial u_1}{\partial x_1} + \frac{\partial v_1}{\partial y_1} = 0 \quad , \tag{3-2}$$

$$u_1 \frac{\partial u_1}{\partial x_1} + v_1 \frac{\partial u_1}{\partial y_1} = \frac{1}{Re} \frac{\partial}{\partial y_1} \left(\frac{\nu_e}{\nu} \frac{\partial u_1}{\partial y_1} \right) + U_1 \frac{dU_1}{dx} \quad , \tag{3-3}$$

$$\frac{\nu_e}{\nu} = \begin{cases} \left(\frac{\nu_e}{\nu}\right)_i = 1 + Re \left\{0.4\, y_1 \left[1 - \exp\left(\frac{-y_1 L}{A}\right)\right]\right\} \left|\frac{\partial u_1}{\partial y_1}\right|_{\gamma_t} \\ \left(\frac{\nu_e}{\nu}\right)_0 = 1 + 0.0168\, R_{\delta^*} U_1(x_1)\gamma\gamma_t \end{cases} \tag{3-4}$$

$$u_1(x_1, 0) = 0 \quad , \quad v_1(x_1, 0) = 0 \quad , \quad u_1(x_1, y_1 \to \infty) \to U_1(x_1) \quad , \tag{3-5}$$

$$u_1(0, y_1) = u_0(y(y_1))/U_\infty \quad , \tag{3-6}$$

where $Re \equiv U_\infty L/\nu$ is the Reynolds number while $R_{\delta^*} \equiv U_\infty \delta^*/\nu$ is the Reynolds number based on the displacement thickness δ^*.

By use of another transformation the transformed equations can be made independent of the Reynolds number and the boundary conditions the same for all conceivable problems of the class considered. Let

$$x_2 = \int_0^{x_1} U_1(s)\, ds \quad , \quad y_2 = Re^{\frac{1}{2}} U_1(x_1) y_1 \quad , \tag{3-7}$$

$$u_2(x_2, y_2) = \frac{u_1(x_1, y_1)}{U_1(x_1)} \quad , \quad U_2(x_2) = U_1(x_1) \quad ,$$

$$v_1(x_1, y_1) = Re^{-\frac{1}{2}} U_1(x_1)\left[v_2(x_2, y_2) - y_2\, u_2 \frac{d \ln U_2}{d x_2}\right] .$$

Then equations (3-2)-(3-6) become

$$\frac{\partial u_2}{\partial x_2} + \frac{\partial v_2}{\partial y_2} = 0 \quad , \tag{3-8}$$

$$u_2 \frac{\partial u_2}{\partial x_2} + v_2 \frac{\partial u_2}{\partial y_2} = \frac{\partial}{\partial y_2}\left(\frac{\nu_e}{\nu} \frac{\partial u_2}{\partial y_2}\right) + (1 - u_2^2) \frac{d \ln U_2}{d x_2} \quad , \tag{3-9}$$

$$\frac{\nu_e}{\nu} = \begin{cases} \dfrac{\nu_e}{\nu} = \left(\dfrac{\nu_e}{\nu}\right)_i = 1 + Re^{\frac{1}{2}}\{0.4\, y_2\, [1 - \exp\left(-\dfrac{y_2 L}{A Re^{\frac{1}{2}} U_2(x_2)}\right)]\}^2 \left|\dfrac{\partial u_2}{\partial y_2}\right| \gamma\gamma_t \\ \left(\dfrac{\nu_e}{\nu}\right)_0 = 1 + 0.0168\, R_{\delta^*} U_2(x_2) \gamma\gamma_t \quad , \end{cases} \tag{3-10}$$

$$u_2(x_2, 0) = 0 \quad , \quad v_2(x_2, 0) = 0 \quad , \quad u_2(x_2, y_2 \to \infty) \to 1 \quad , \tag{3-11}$$

$$u_2(0, y_2) = u_0(y(y_2))/U_2(0)U_\infty \quad . \tag{3-12}$$

It is known that the number of dependent variables can be reduced by one if the Von Mises transformation is introduced (e.g. Yih, [12]). One can introduce a stream function $\psi(x_2, y_2)$ to satisfy the continuity equation (3-8), with

$$u_2(x_2, y_2) = \frac{\partial \psi_2(x_2, y_2)}{\partial y_2} \quad , \quad v_2(x_2, y_2) = - \frac{\partial \psi_2(x_2, y_2)}{\partial x_2} \, . \tag{3-13}$$

Then in the Von Mises transformation the stream function ψ_2 is used as the independent variable corresponding to y_2. Let

$$\psi_3(x_2, y_2) = \psi_2(x_2, y_2) = \int_0^{y_2} u_2(x_2, s)\, ds \, , \quad x_3 = x_2 \, , \tag{3-14}$$

$$u_3(x_3, \psi_3) = u_2(x_2, y_2) \, , \quad U_3(x_3) = U_2(x_2) \, .$$

Equations (3-8)-(3-12) become

$$u_3 \frac{\partial u_3}{\partial x_3} = \frac{\nu_e}{\nu} u_3 \left(\frac{\partial u_3}{\partial \psi_3}\right)^2 + u_3 \frac{\partial}{\partial \psi_3} \left(\frac{\nu_e}{\nu} \frac{\partial u_3}{\partial \psi_3} \right) + (1 - u_3^2) \frac{d \ln U_3(x_3)}{d x_3} \, , \tag{3-15}$$

$$\frac{\nu_e}{\nu} = \begin{cases} \left(\frac{\nu_e}{\nu}\right)_i = 1 + Re^{\frac{1}{2}} u_3 \left|\frac{\partial u_3}{\partial \psi_3}\right| \{0.4\, y_2(\psi_3)[1 - \exp(\frac{-y_2(\psi_3)L}{A\, Re^{\frac{1}{2}} U_3(x_3)})]\}^2 \gamma_t \, , \\ \left(\frac{\nu_e}{\nu}\right)_0 = 1 + 0.0168\, R_{\delta^*}\, U_3(x_3) \gamma \gamma_t \, , \end{cases} \tag{3-16}$$

$$u_3(x_3, 0) = 0 \quad , \quad u_3(x_3, \psi_3 \to \infty) \to 1 \quad , \tag{3-17}$$

$$u_3(0, \psi_3) = u_0(y(\psi_3))/U_2(0)U_\infty \quad . \tag{3-18}$$

Furthermore, if one introduces the new function

$$w_3(x_3, \psi_3) = u_3^2(x_3, y_3) \quad , \tag{3-19}$$

one obtains

$$\frac{\partial w_3}{\partial x_3} = w_3^{\frac{1}{2}} \frac{\partial}{\partial \psi_3}\left(\frac{\nu_e}{\nu} \frac{\partial w_3}{\partial \psi_3}\right) + 2(1 - w_3) \frac{d \ln U_3(x_3)}{d x_3} \quad , \tag{3-20}$$

$$\frac{\nu_e}{\nu} = \begin{cases} \left(\frac{\nu_e}{\nu}\right)_i = 1 + \tfrac{1}{2} Re^{\frac{1}{2}} \{0.4\, y_2(\psi_3)[1 - \exp(\frac{-\, y_2(\psi_3)\, L}{AR_e^{\frac{1}{2}} U_3(x_3)})]\}^2 \left|\frac{\partial w_3}{\partial \psi_3}\right|_{\gamma_t} \\ \left(\frac{\nu_e}{\nu}\right)_0 = 1 + 0.0168\, R_{\delta^*} U_3(x_3) \gamma\gamma_t \quad , \end{cases} \tag{3-21}$$

$$w_3(x_3, 0) = 0 \quad , \quad w_3(x_3, \psi_3 \to \infty) \to 1 \quad , \tag{3-22}$$

$$w_3(0, \psi_3) = w_0(\psi_3) \quad . \tag{3-23}$$

For a boundary layer profile whose development with respect to y_1 starts with the linear term, the independent variable ψ_3 is inconvenient to use for a function which is analytic in y_1 and not analytic in terms of ψ_3 (Guderley and Hsu, [13]). This motivates the following transformation:

$$\begin{aligned} &\eta_4 = \psi_3^{\frac{1}{2}} \quad , \quad x_4 = x_3 \quad , \\ &w_4(x_4, \eta_4) = w_3(x_3, \eta_3) \quad , \quad U_4(x_4) = U_3(x_3) \quad , \end{aligned} \tag{3-24}$$

Hence, one finds

$$\frac{\partial w_4}{\partial x_4} = \frac{w_4^{\frac{1}{2}}}{4}\left[\frac{1}{\eta^2 4} \frac{\partial}{\partial \eta_4}\left(\frac{\nu_e}{\nu} \frac{\partial w_4}{\partial \eta_4}\right) - \frac{1}{\eta_4^3} \frac{\nu_e}{\nu} \frac{\partial w_4}{\partial \eta_4}\right] + 2(1 - w_4) \frac{d \ln U_4(x_4)}{d x_4} \quad , \tag{3-25}$$

$$\frac{\nu_e}{\nu} = \begin{cases} \left(\frac{\nu_e}{\nu}\right)_i = 1 + \tfrac{1}{4}\,Re^{\frac{1}{2}}\{0.4\,y_2(\eta_4)[1 - \exp(-\frac{y_2(\eta_4)L}{ARe^{\frac{1}{2}}U_4(x_4)})]\}^2\frac{1}{\eta_4}\left|\frac{\partial w_4}{\partial \eta_4}\right|\gamma\gamma_t \ , \\ \left(\frac{\nu_e}{\nu}\right)_0 = 1 + 0.0168\,R_{\delta^*}U_3(x_3)\gamma\gamma_t \ , \end{cases} \tag{3-26}$$

$$w_4(x_4, 0) = 0 \ , \quad w_4(x_4, \eta_4 \to \infty) \to 1 \ , \tag{3-27}$$

$$w_4(0, \eta_4) = w_0(\eta_4) \ . \tag{3-28}$$

For any numerical method of solution, it is desirable to have the transformed boundary layer thickness remain approximately the same order of magnitude through the entire flow region. The rate of growth of a turbulent boundary layer is not known; however, for laminar boundary flows the application of the Falkner-Skan transformation seems to maintain a boundary layer thickness of the same order throughout the entire flow region (Schlichting, [14]). Therefore, one hopes the Falkner-Skan transformation may somewhat decrease the growth rate of the turbulent boundary layer. The Falkner-Skan transformation is given by

$$\eta = x_4^{-\frac{1}{4}}\,\eta_4 \ , \quad \xi = \int_{\varepsilon}^{x_4} \frac{ds}{s} \ , \tag{3-29}$$

$$w(\xi, \eta) = w_4(x_4, \eta_4) \ , \quad W(\xi) = U_4(x_4) \ ,$$

where ε is a small constant introduced to overcome the singularity resulted from a coordinate transformation. Then equations (3-25)-(3-28) become

$$\frac{\partial w}{\partial \xi} = \frac{w^{\frac{1}{2}}}{4}\left[\frac{1}{\eta^2}\frac{\partial}{\partial \eta}\left(\frac{\nu_e}{\nu}\frac{\partial w}{\partial \eta}\right) - \frac{1}{\eta^3}\frac{\partial w}{\partial \eta}\frac{\nu_e}{\nu}\right] + \frac{\eta}{4}\frac{\partial w}{\partial \eta} + 2(1 - w)\frac{d \ln W(\xi)}{d \xi} \ , \tag{3-30}$$

$$\frac{\nu_e}{\nu} = \begin{cases} \left(\frac{\nu_e}{\nu}\right)_i = 1 + 0.25\left(\frac{Re}{\varepsilon e^{\xi}}\right)^{\frac{1}{2}}\{0.4\, y_2(\eta)[1 - \exp\left(-\frac{y_2(\eta)L}{ARe^{\frac{1}{2}}W(\xi)}\right)]\}^2 \frac{1}{\eta}\left|\frac{\partial}{\partial\eta}\right|^{\gamma_t} \\ \\ \left(\frac{\nu_e}{\nu}\right)_0 = 1 + 0.0168\, R_{\delta^*}\, W(\xi)^{\gamma\gamma_t} \quad , \end{cases} \tag{3-31}$$

$$w(\xi, 0) = 0 \quad , \quad w(\xi, \eta\to\infty) \to 1 \quad , \tag{3-32}$$

$$w(0, \eta) = w_0(\eta) \quad . \tag{3-33}$$

In the present formulation, the dependent variable $w(\xi, \eta)$ is the square of the dimensionless velocity. Because of the homogeneous boundary conditions, equation (3-11) and the transformation, equation (3-14) and (3-19), one has, for sufficiently small value of η,

$$w(\xi, \eta) = O(\eta^2) \quad , \tag{3-34}$$

which implies that

$$\left.\frac{\partial w}{\partial \eta}\right|_{\eta=0} = 0 \quad . \tag{3-35}$$

Furthermore, the asymptotic behavior of a boundary-layer profile implies that

$$\lim_{\eta\to\infty} \frac{\partial w}{\partial \eta} = 0 \quad . \tag{3-36}$$

For application of a numerical method, the boundary condition at infinity must be imposed at a finite but sufficiently large distance H. The proper choice of H is in general crucial to the efficiency of a given numerical scheme as well as to the accuracy of the results obtained. Hence, for a selected H, the initial-boundary value problem to be

numerically solved is governed by

$$\frac{\partial w}{\partial \xi} = R_1(w) \quad , \tag{3-37}$$

$$\frac{\nu_e}{\nu} = \begin{cases} \left(\frac{\nu_e}{\nu}\right)_i = 1 + 0.25\left(\frac{Re}{\varepsilon e^{\xi}}\right)^{\frac{1}{2}}\{0.4\, y_2(\eta)[1 - \exp(\frac{-y_2(\eta)L}{ARe^{\frac{1}{2}}W(\xi)})]\}^2\left|\frac{\partial w}{\partial \eta}\right|\gamma_t \frac{1}{\eta} \\ \left(\frac{\nu_e}{\nu}\right)_0 = 1 + 0.0168\, R_{\delta^*} W(\xi)\gamma\gamma_t \quad , \end{cases} \tag{3-38}$$

$$\text{at } \eta = 0 \ : \ w = 0 \quad , \tag{3-39}$$

$$\text{at } \eta = H \ : \ w = 1 \quad , \tag{3-40}$$

$$\text{at } \xi = 0 \ : \ w = w_0(\eta) \quad , \tag{3-41}$$

where the nonlinear operator $R_1(w)$ is given by the right hand side of equation (3-30). The additional boundary conditions, equation (3-35) and (3-36) are

$$\frac{\partial w}{\partial \eta} = 0 \qquad \text{at } \eta = 0 \text{ and at } \eta = H \tag{3-42}$$

which are important and useful in the spline fit approximation.

Following the transformations given by equations (3-1), (3-7), (3-14), (3-19), (3-24) and (3-29), the shear stress is given by

$$\tau_w(\xi) = \frac{\rho(U_\infty W(\xi))^2}{4(Re\varepsilon e^{\xi})^{\frac{1}{2}}}\left(\frac{1}{\eta}\frac{\partial w}{\partial \eta}\right)_{\eta = 0} \quad . \tag{3-43}$$

One notes from equation (3-35) that

$$\left(\frac{1}{\eta}\frac{\partial w}{\partial \eta}\right)_{\eta=0} = \left.\frac{\partial^2 w}{\partial \eta^2}\right|_{\eta=0} \quad . \tag{3-44}$$

Consequently, the local skin-friction coefficient, C_f defined by

equation (2-22), becomes

$$C_f = \frac{1}{2(Re\varepsilon e^{\xi})^{\frac{1}{2}}} \left.\frac{\partial^2 w}{\partial \eta^2}\right|_{\eta=0} . \tag{3-45}$$

The system of governing equations (3-37)-(3-41) will be used to investigate the development and applicability of a finite element differential method in which the unknown function $w(\xi, \eta)$ at a streamwise station ξ is represented by the classical cubic spline. Some of the important variables and parameters which must be evaluated in the course of computation are

$$y_2 = (\varepsilon e^{\xi})^{\frac{1}{2}} \int_0^{\eta} \frac{2s}{w^{\frac{1}{2}}} ds , \tag{3-46}$$

$$\gamma = [1 + 5.5(\frac{\eta}{\eta_H})^6]^{-1} , \tag{3-47}$$

$$\gamma_t = 1 - \exp[-\frac{Re^2 W^2(\xi)\varepsilon^2}{1200} R_{x_{tr}}^{-1.34} \int_{e^{\xi}tr}^{e^{\xi}} \frac{ds}{W(s)} \int_{e^{\xi}tr}^{e^{\xi}} \frac{ds}{W^2(s)}] \tag{3-48}$$

$$R_{x_{tr}} = Re\, W(\xi)\varepsilon \int_0^{e^{\xi}tr} \frac{ds}{W(s)} , \tag{3-49}$$

$$R_{\delta^*} = (Re\ \varepsilon e^{\xi})^{\frac{1}{2}} [\int_0^H (\frac{2\eta}{w^{\frac{1}{2}}} - 2\eta)\, d\eta] . \tag{3-50}$$

CHAPTER IV
CLASSICAL SPLINE APPROXIMATION

In approximating a mathematical function, a spline function will usually provide closer and smoother approximations to the function and its low-order derivatives than a polynomial (Greville, [15]). The amount of computation involved is not materially greater than that required in a polynomial. In addition, the spline functions possess certain impressive optimal properties such as minimum norm, strong convergence and best approximation (Ahlberg et al. [16]).

A spline function is a function whose graph is a composite curve made up of a number of polynomial arcs of a given degree fitted together in such a way that the junctions of successive arcs are as smooth as they can be made without going to a single polynomial over the entire range. Mathematically, the spline function can be defined as follows: Let $\upsilon = \eta_0, \eta_1, \ldots, \eta_n, \eta_{n+1} = H$ be a strictly increasing sequence of real numbers (called nodes of the spline function). Then a spline function of degree m with the nodes $\eta_0, \eta_1, \ldots, \eta_n, \eta_{n+1}$ is a function $s(\eta)$ satisfying the following two conditions:

(1) In each interval (η_j, η_{j+1}) $(i = 0, 1, \ldots, n)$ $S(\eta)$ is given by a polynomial of degree m.

(2) $S(\eta)$ and its derivatives of order 1, 2, ..., m - 1 are continuous over the region (0, H).

A spline function, in general, may be represented in two distinct, but completely equivalent ways. The choice of the representation

materially affects the formulation of the problem and its ease of solution.

The first representation is referred to as the piecewise polynomial representation; it simply uses different polynomials of the same degree m, one for each interval. This formulation can be written as

$$S_j(\eta) = \sum_{i=1}^{m} C_{ij}(\eta - \eta_{j-i})^i, \quad \eta \in (\eta_{j-i}, \eta_j) \; j = 1, 2, \ldots, \eta + 1, \tag{4-1}$$

$S_j(\eta)$ represents the polynomial of degree m in the jth interval. C_{ij} are the coefficients for the polynomials and are determined by applying the continuity conditions at internal nodes and boundary conditions at the two extreme nodes. When this formulation is used, the continuity conditions are explicitly part of the problem to be programmed. This representation is easily understood and the computations involved are simple and straightforward.

The second representation is formed by a set of basis functions. A spline function represented by a set of basis functions is called a B-spline. The B-spline may be written as

$$S(\eta) = \sum_{i=1}^{\eta+m+1} d_i \, B_{i,m}(\eta) \quad , \tag{4-2}$$

where $B_{i,m}(\eta)$ is the so-called "compact support basis" and d_i are the coefficients of the B-spline. When a B-spline is used to approximate the solution of a differential equation, it leads to well-behaved matrices in addition to having built-in continuity. The drawback of this representation is that B-splines are not simply related to elementary functions, and must be evaluated, using their definition as a divided

difference of the truncated power function. Further reference to B-splines and their properties is given elsewhere (De Boor, [17]).

In general, cubic spline functions with m = 3 are the most useful and interesting ones because of their easy application. The first representation of the cubic spline function will be used to approximate the transformed velocity profile in this study.

Cubic spline functions have been effectively applied to some fluid flow problems. Panton and Sallee [18] have considered heat condition and laminar boundary layer flow problems using both point collocation and integral methods, in which assumed solutions were represented by B-splines. Rubin and Khosla [19], [8] have investigated in detail the applicability of cubic splines for Burgers equation, potential flow and boundary layer flow problems using higher-order collocation methods. Hsu (1976) has studied the classical cubic spline with the subdomain collocation method for laminar boundary layer flows past a submerged body. Furthermore, Inoue, Kuromaru and Yamaguchi [20] made use of a cubic spline in solving a potential flow problem.

In the proposed method of solution the transformed boundary layer region is first divided into n + 1 strips of unequal size which are parallel to the fixed boundary $\eta = 0$. The unknown solution $w(\xi, \eta)$ at a streamwise station ξ is approximated by the classical cubic spline. The choice of the approximation seems to be very well suited for the laminar boundary layer flow region since the governing equations are of second order in η and the cubic spline does satisfy continuity of the dependent variable, its slope and curvature at the joint nodes. Therefore, it is expected that highly accurate results will be obtained in

that region. When the approximation is applied to the transitional and turbulent flow region, the slope of the eddy viscosity which is not continuous at the matching point because of the closure model, may introduce some difficulties and require special measures in approximations.

Let $f(\xi, \eta)$ be the function to be approximated by a cubic spline function in the interval $0 \leq \eta \leq H$. Assume that the interval is divided into $n + 1$ elements with the nodal points

$$0 = \eta_0 < \eta_1 < \ldots < \eta_n < \eta_{n+1} = H$$

Denote the function $f(\xi,\eta)$ and its first and second derivatives with respect to η evaluated at the nodal points η_i as

$$f(\xi, \eta_i) = f_i(\xi), \quad \left.\frac{\partial f}{\partial \eta}\right|_{\eta=\eta_i} = f_i'(\xi), \quad \left.\frac{\partial^2 f}{\partial \eta^2}\right|_{\eta=\eta_i} = f_i''(\xi) . \qquad (4\text{-}3)$$

Moreover, for an ith element the local coordinate z and the element size h_i are defined by

$$z = \eta - \eta_{i-1} , \qquad (4\text{-}4)$$

$$0 \leq z \leq h_i = \eta_i - \eta_{i-1} , \quad \text{for } i = 1 , \ldots , n + 1 .$$

Use of the local coordinate instead of the global coordinate simplifies much of the formulation and computation. Let $g_i(\xi, z)$ be the cubic polynomial approximating $f(\xi, \eta)$ in the ith element. Then the continuity of curvature at nodes η_{i-1} and η_i indicates that

$$\frac{\partial^2 g_i}{\partial z^2} = \frac{1}{h_i} [(h_i - z) f_{i-1}''(\xi) + z f_i''(\xi)] . \qquad (4\text{-}5)$$

Integrating equation (4-5) twice with respect to z and applying the conditions $g_i(\xi, 0) = f_{i-1}(\xi)$ and $g_i(\xi, h_i) = f_i(\xi)$ one obtains the cubic polynomial for the ith element

$$g_i(\xi, z) = \frac{[(h_i - z)^3 + h_i^2(z - h_i)]\, f''_{i-1}(\xi) + [z^3 - h_i^2 z]\, f''_i(\xi)}{6 h_i} + \frac{[(h_i - z) f_{i-1}(\xi) + z f_i(\xi)]}{h_i} . \tag{4-6}$$

Next, evaluating the slope at the extreme nodes η_0 and η_{n+1} and satisfying the continuity of slope at joint nodes, that is,

$$\left.\frac{\partial g_i(\xi, z)}{\partial z}\right|_{z=h_i} = \left.\frac{\partial g_{i+1}(\xi, z)}{\partial z}\right|_{z=0} , \tag{4-7}$$

for i = 1, 2, ... , n, one obtains the following system of (n + 2) linear algebraic equations:

$$\begin{aligned}
&\frac{h_1}{3} f''_0 + \frac{h_1}{6} f''_1 = -\frac{f_0}{h_1} + \frac{f_1}{h_1} - f'_0 , \\
&\frac{h_i}{6} f''_{i-1} + \frac{h_i + h_{i+1}}{3} f''_i + \frac{h_{i+1}}{6} f''_{i+1} = \frac{f_{i-1}}{h_i} - \left(\frac{1}{h_i} + \frac{1}{h_{i+1}}\right) f_i + \frac{f_{i+1}}{h_{i+1}} , \\
&\frac{h_{n+1}}{6} f''_n + \frac{h_{n+1}}{3} f''_{n+1} = \frac{f_n}{h_{n+1}} - \frac{f_{n+1}}{h_{n+1}} + f'_{n+1} .
\end{aligned} \tag{4-8}$$

These equations can be put into the matrix form

$$[B]\{f''\} = [c]\{f\} + \{f'\} , \tag{4-9}$$

where both [B] and [c] are symmetric, tridiagonal, (n + 2) by (n + 2)

constant matrices. The vectors {f''} and {f} have n + 2 elements but {f'} has only two elements f'_0 and f'_{n+1}. It is clear that the inverse of [B] does exist and hence one has

$$[f''] = [B]^{-1}\,[c]\,\{f\} + [B]^{-1}\{f'\}. \tag{4-10}$$

Accordingly, one has

$$f'_i{}''(\xi) = \sum_{j=0}^{n+1} \alpha_{ij} f_j(\xi) - \beta_{i,0}\, f'_0(\xi) + \beta_{i,n+1}\, f'_{n+1}(\xi), \tag{4-11}$$

where the constants α_{ij} are elements of $[B]^{-1}[c]$ and $\beta_{i,j}$ are elements of the inverse of [B].

In accordance with equation (3-42) if one assumes that the slopes at the extreme nodes η_0 and η_{n+1} are zero, one obtains

$$f'_i{}''(\xi) = \sum_{j=0}^{n+1} \alpha_{ij} f_j(\xi) \quad , \quad i = 0, 1, \ldots , n, n+1. \tag{4-12}$$

This implies that the second derivative at each node depends linearly upon all the nodal functions $f_j(\xi)$; however, $f'_i{}''(\xi)$ is generally influenced by the nodal functions $f_j(\xi)$ in the neighborhood of the ith node. For example, when the element size distribution is the following:

$$H = 2.5 \ , \ n = 3 \ , \ h_i = /0.2,\ 0.3,\ 0.5,\ 1.5/ \ ,$$

α_{ij} can be determined and written in a matrix form as

$$[\alpha_{i,j}] = \begin{bmatrix} -101.76 & 115.99 & -15.86 & 1.73 & -0.11 \\ 53.51 & -81.98 & 31.71 & -3.46 & 0.22 \\ -10.54 & 29.28 & -28.47 & 10.38 & -0.65 \\ 1.62 & -4.50 & 8.07 & -7.14 & 1.95 \\ -0.81 & 2.25 & -4.04 & 4.90 & -2.31 \end{bmatrix} \tag{4-13}$$

which clearly indicates the weight of $f_j(\xi)$ on the curvature $f_i''(\xi)$.

Substituting equation (4-12) into equation (4-6) gives

$$g_i(\xi, z) = \sum_{j=0}^{n+1} a_{ij}(z)\, f_j(\xi) \quad , \tag{4-14}$$

where $a_{ij}(z)$ is a known polynomial of degree three in z and is given by

$$a_{ij}(z) = \frac{[(h_i - z)^3 + h_i^2(z - h_i)]\, \alpha_{i-1,j} + [z^3 - h_i{}^2 z]\alpha_{ij}}{6\, h_i} + \frac{h_i - z}{h_i}\, \delta_{i-1,j} + \frac{z}{h_i}\, \delta_{i,j} \quad . \tag{4-15}$$

Here $\delta_{i,j}$ is the Kronecker delta. Therefore, the classical spline approximating the function $f(\xi, \eta)$ is

$$s(\xi, \eta) = \sum_{i=1}^{n+1} \delta_i\, g_i(\xi, z) \quad , \tag{4-16}$$

where $\delta_i = 1$ when $\eta_{i-1} \le \eta \le \eta_i$, otherwise $\delta_i = 0$.

CHAPTER V
METHOD OF SOLUTION

Natural variational principles do not exist for boundary layer flow problems and hence formulation of the finite element method should be based on the governing equations. This approach is categorized as the weighted residual method. The weighted residual method is a mathematical means of finding approximate solutions to differential equations. One of its most attractive features is that this method is applicable to nonlinear and non-self-adjoint problems. For a given differential equation and associated boundary and initial conditions, the general approach of the weighted residual method is to assume a trial solution whose functional dependence is chosen, but includes undetermined functions. The latter are found by requiring that the trial solution satisfy the differential equations in some specified approximate sense.

In the proposed numerical method for solution of equations (3-37)-(3-41), the boundary layer flow problem, a subdomain collocation method, one of the weighted residual methods, is employed to reduce the governing partial differential equations into a system of first order, nonlinear, ordinary differential equations. The reduced initial value problem is then numerically integrated to provide the solution.

For the spline approximation of $w(\xi, \eta)$ at a given streamwise station ξ, the interval $0 \leq \eta \leq H$ is divided into $n + 1$ elements with nodes at $0 = \eta_0 < \eta_1 < \ldots\ldots < \eta_n < \eta_{n+1} = H$ and element size $h_i = \eta_i - \eta_{i-1}$

for i=1, ... , n+1. If one denotes the unknown function $w(\xi, \eta)$, and its first and second derivatives at the ith node as

$$w(\xi, \eta_i) = w_i(\xi) \ , \quad \left.\frac{\partial w}{\partial \eta}\right|_{\eta=\eta_i} = w_i'(\xi) \ , \quad \left.\frac{\partial^2 w}{\partial \eta^2}\right|_{\eta=\eta_i} = w_i''(\xi) \ , \quad (5\text{-}1)$$

and also lets $\bar{w}_i(\xi, z)$ be the cubic polynomial approximating $w(\xi, \eta)$ in the ith element, then the assumed solution for the weighted residual is the sum of the cubics and can be written as

$$w(\xi, \eta) = \sum_{i=1}^{n+1} \delta_i \, \bar{w}_i(\xi, z) \ , \quad (5\text{-}2)$$

where

$$\delta_i = \begin{cases} 1, & \text{when } \eta_{i-1} < \eta < \eta_i \\ 0, & \text{otherwise} \end{cases} \ , \quad z = \eta - \eta_{i-1} \ .$$

As a result of spline approximation, equations (4-5)-(4-12), the assumed solution can be written as

$$w(\xi, \eta) = \sum_{j=0}^{n+1} \left(\sum_{i=1}^{n+1} \delta_i \, a_{ij}(z) \right) w_j(\xi) \ , \quad (5\text{-}3)$$

in which $a_{ij}(z)$ is given by equation (4-14). The quantities inside the parentheses are called shape functions, which are known polynomials of degree three in z.

The substitution of the assumed solution, equation (5-3), into the governing equation (3-37) and application of the weighted residual method gives

$$\int_0^H \gamma_j(\eta) \frac{\partial w}{\partial \xi} \, d\eta = \int_0^H \gamma_j(\eta) \, R_1(w) \, d\eta \ , \quad (5\text{-}4)$$

where $\gamma_j(\eta)$ are the weighting functions and the nonlinear operator $R_1(w)$ is given by the right hand side of equation (3-30). Because of the boundary conditions given by equation (3-32), there are only n values of $w_j(\xi)$ for $j = 1, \ldots, n$ in equation (5-3) to be determined. Thus one needs n equations for n unknowns; consequently, it requires a choice of n weighting functions to be used in equation (5-4). The error made by the spline approximation at each interior nodal point is mostly propagated to the neighboring intervals (Hildebrand, [21]). This suggests that the weighting functions $\gamma_j(\eta)$ should be chosen so that the residuals will be distributed to both sides of the nodal point in some sense. For simplicity the weighting functions employed in this study are boxcar functions of the form

$$\gamma_j(\eta) = \begin{cases} 1, & \text{when } \eta_{j-1} \le \eta \le \eta_{j+1} \\ 0, & \text{otherwise} \end{cases} . \qquad (5\text{-}5)$$

This choice implies that the subdomain collocation method is employed in the approximate procedure which forces the residual to be uniformly distributed over the two neighboring elements for each interior nodal point. Equation (5-4) incorporated with equations (5-2) and (5-5), therefore, gives the following system of n equations

$$\int_0^{h_i} \frac{\partial \bar{w}_i}{\partial \xi}\, dz + \int_0^{h_{i+1}} \frac{\partial \bar{w}_{i+1}}{\partial \xi}\, dz = \int_0^{h_i} R_1(\bar{w}_i)dz + \int_0^{h_{i+1}} R_1(\bar{w}_{i+1})dz, \quad (5\text{-}6)$$

for $i = 1, 2, \ldots, n$. The substitution of the explicit expression for the cubic polynomial $\bar{w}_i(\xi, z)$ in equation (4-14) then gives a system of n first order nonlinear ordinary differential equations in $w_1(\xi)$, $w_2(\xi)$, $\ldots\ldots$, $w_n(\xi)$, which can be expressed in matrix form as

$$[Q]\ \{\frac{dw}{d\xi}\} = \{\gamma_1(\xi, w)\} \tag{5-7}$$

or

$$\{\frac{dw}{d\xi}\} = [Q]^{-1}\{\gamma_1(\xi,w)\} \tag{5-8}$$

where [Q] is a nonsingular n by n constant matrix with its elements given by

$$q_{i,j} = -\frac{1}{24}[h_i^3(\alpha_{i,j+1} + \alpha_{i+1,j+1}) + h_{i+1}^3(\alpha_{i+1,j+1} + \alpha_{i+2,j+1})]$$
$$+ \delta_{i-1,j}\frac{h_i}{2} + \delta_{i,j}\frac{(h_i + h_{i+1})}{2} + \delta_{i+1,j}\frac{h_{i+1}}{2} . \tag{5-9}$$

The elements of the n dimensional vector {w} are $w_1(\xi)$, $w_2(\xi)$, ... , $w_n(\xi)$, and those of $\{\gamma_1(\xi,w)\}$ are the integrals of nonlinear functions of the elements of {w} given by the right hand side of equation (3-30), that is,

$$R_1(w) = \frac{w^{\frac{1}{2}}}{4}[\frac{1}{\eta^2}\frac{\partial}{\partial\eta}(\frac{\nu_e}{\nu}\frac{\partial w}{\partial\eta}) - \frac{1}{\eta^3}\frac{\partial w}{\partial\eta}\frac{\nu_e}{\nu})] + \frac{\eta}{4}\frac{\partial w}{\partial\eta} + 2(1 - w)\frac{d\ \ln\ W\ (\xi)}{d\xi} . \tag{5-10}$$

With the given initial condition, equation (3-41), which is discretized at the interior nodes, the system of n equations, (5-8), can be integrated numerically to provide the solution.

CHAPTER VI
COMPUTATIONAL METHODOLOGY

The computational work involved in the proposed method appears very complicated and laborious. However, the computations can be simplified and reduced to a minimum by developing the numerical algorithm carefully.

For a given boundary layer flow problem, the constant matrices [B], [C] and [Q] in equations (4-9) and (5-7) are determined after the flow region has been discretized into n + 1 elements in the η direction. The question of finding the inverse of the matrices [B] and [Q] is of primary importance. There are many methods whereby the inverse of a matrix can be determined. In this study the Gauss-Jordan elimination method has been used, since the difference in computer time between the Gauss-Jordan elimination method and the Gauss elimination method is insignificant in finding the inverse of matrices such as [B] and [Q]. For the mathematical basis of the Gauss-Jordan elimination and a FORTRAN program see Hornbeck [22]).

The main difference between the proposed method and the finite difference method is that integrations are required using the finite element approach. The right hand side of equation (5-7) must be evaluated at each integration step. Unfortunately, an explicit expression for elements of $\{r_1(\xi, w)\}$ cannot be obtained due to the fact that the operator $R_1(w)$ involves the square root of the dependent variable. Hence, an approximation technique must be employed for evaluating the integrals

on the right hand side of equation (5-6). Two different approximation techniques had been investigated for the laminar boundary layer flow problem (i.e. $\frac{\nu_e}{\nu} = 1$) (Hsu, 1976). The first approximation utilizes a Taylor series expansion. The manipulation involved in this approximation is rather tedious and cumbersome; hence, this approach is not suitable for the complex turbulent boundary layer flows. An alternative approach considered was to evaluate those integrals numerically using a Gauss-Legendre quadrature formula, which is generally capable of supplying comparable accuracy with fewer ordinates compared with numerical integration formulas such as the Simpson's rule and the trapezoidal rule. This latter approach is employed in the present study.

The Gauss-Legendre quadrature formula is given by

$$\int_{-1}^{1} F(\zeta)d\zeta = \sum_{m=1}^{M} A_m^{(M)} \; F(\zeta_m^{(M)}) \; , \tag{6-1}$$

where the set of weighting coefficients $A_m^{(M)}$ and roots $\zeta_m^{(M)}$, for a given M are obtained in such a way that the quadrature formula is exact whenever the integrand $F(\zeta)$ is a polynomial of degree less than or equal to 2M - 1. For reference, see Krylov [23]). For actual evaluations of the integrals given in equation (5-6), one notes that the simple transformation of the variable

$$z = \frac{h_i}{2} (1 + \zeta) \tag{6-2}$$

gives the relation

$$\int_0^{h_i} \bar{F}(z) \; dz = \frac{h_i}{2} \int_{-1}^{1} F(\zeta) \; d\zeta = \frac{h_i}{2} \sum_{m=1}^{M} A_m^{(M)} \; F(\zeta_m^{(M)}) \; . \tag{6-3}$$

For turbulent boundary-layer flow problems the values of M = 6 and M = 4 have been tested. The results obtained using M = 6 and M = 4 are almost the same. This implies that M = 4 can give acceptable accuracy.

When one comes to evaluate the functional values $F(\zeta_m^{(M)})$ another difficulty arises because F is not an explicit function of z, due to the equation (3-46). Consequently, a simple tabulation and interpolation technique must be employed in determining the value of y_2 for a given η at each streamwise station ξ. The interpolation process is based on the polynomial of an assigned degree constructed by points which are close to the value for which interpolation is desired. This interpolation is carried out by a general purpose function subprogram ATKN (X, Y, N, k, XI), which is listed in appendix B.

The reduced initial value problem, equation (5-8), can be solved by a numerical integration method. Hamming's 4th order predictor-corrector method (Ralston, [24]) and Gear's stiff method (Gear, [25]) are employed to solve equation (5-8) in this study.

The solution obtained by Hamming's 4th order predictor-corrector method shows that the integration step size is quite small so that the efficiency of the solution method is deteriorated. This motivates the investigation on the degree of stiffness associated with the reduced initial value problem. Because of the nonlinearity of equation (5-8), one has to examine the results obtained using the Hamming method to determine the degree of stiffness of the equations. The reduced initial value problem is indeed very stiff. The typical step size required is extremely small for the solution behavior obtained. Accordingly, Gear's stiff method which has been shown to be very efficient for stiff

equations (Hindmarsh, [26]) is utilized to solve the reduced initial value problem.

The University of Florida Amdahl 470 V/6-II and IBM 3033N computers have been used to perform the numerical experiments in double precision computations. Cases I to IV have been performed by the Amdahl 470 V/6-II. Cases V to XII have been performed by the IBM 3033N.

CHAPTER VII
FINDINGS OF PRELIMINARY NUMERICAL EXPERIMENTS

To investigate the applicability as well as the accuracy and efficiency of the solution method for turbulent boundary-layer flows, the turbulent boundary layer flow over a flat plate has been considered for numerical experiments in this study. This flow problem is a severe test for a numerical method, since the last term of the equation (3-30) is zero and consequently, the only forcing function which is related to the eddy viscosity for changing the solution profile in the streamwise direction is implicitly dependent upon the unknown solution. For such a parabolic problem, an accurate initial profile is very essential for accurate results. Any error made in the computed effective eddy viscosity may require a large number of integration steps to correct; moreover, an inaccurate computation for the effective eddy viscosity distribution across the boundary layer at a streamwise station can be detrimental to the solution. Therefore, to numerically solve the governing equations for turbulent flows over a flat plate with a two-layer eddy viscosity model is a great challenge.

In the development of the solution method a problem with a unit Reynolds number of 1×10^6 (U_∞ = 160 ft/sec, $\nu = 1.6 \times 10^{-4}$ ft^2/sec, L = 1 ft) has been chosen for the numerical test. The transitional point from laminar to turbulent flows is specified at the local Reynolds number $Re_x \equiv \frac{Ux}{\nu} = 5.45 \times 10^4$ which had been used by Rubin and Khosla (1977) and corresponds to the transformed variable $\xi_{tr} = \xi = 10.906$. The transitional intermittency factor for flow over a flat plate ($W(\xi) = 1$)

can be obtained from equation (3-48) under the assumption that ε in equation (3-48) is equal to 10^{-6}. The transitional intermittency factor is given by

$$\gamma_t = 1 - \exp\left[-\frac{(e^{\xi} - e^{\xi_{tr}})^2}{1200(e^{\xi_{tr}})^{1.34}}\right] \qquad (7\text{-}1)$$

For application of the method, a boundary condition at infinity must be imposed at a finite but sufficiently large distance H from the fixed boundary. The interval $0 \leq \eta \leq H$ is then divided into a limited number of elements, N, of different sizes, h_i for $i = 1, .., N$, for spline approximations. How to discretize the region considered for a finite element method depends completely on how much is known about the problem. In turbulent boundary layer flows it is known that very steep velocity gradients occur near the wall and approximately zero velocity gradients exist near the edge of the outer boundary layer. From the efficiency view point of the method, a variable grid system is preferred. Thus, small element sizes must be used in the vicinity of the wall in order to obtain an accurate estimation of the wall shear stress, and relatively large element sizes can be used near the edge of the boundary. Since the nature of velocity profiles in turbulent boundary layers is not well understood, the importance and difficulty in choosing the proper or optimal discretization of the flow region is greatly enhanced in this study.

Since the initial profile, in general,is not available in turbulent regions, the integration must be started at a streamwise station in the laminar region where the initial profile can be obtained. An approximate profile to the Blasius equation is used as the initial profile in this study. This transformed approximate profile is

$$w_0(\eta) = [2(\frac{\eta}{H})^2 - 2(\frac{\eta}{H})^3 + (\frac{\eta}{H})^4]^2 \quad . \tag{7-2}$$

For the first numerical experiment, the following finite element model was selected based on experience from computation of laminar boundary layer flows:

case I: H = 7.0, N = 16, h_i = /0.1, 0.2, 0.3, 0.4, 12*0.5/.

The value of H = 7.0 is believed to be large enough for the range of the local Reynolds number to be covered. The integration of the reduced initial value problem, equation (5-8), is started at a streamwise station, $Re_x = 4.8 \times 10^4$, in the laminar flow region with the assumed profile given by equation (7-2) as the initial profile. The average integration step required for an average accuracy of 10^{-6} in the modified Hamming's 4th order predictor-corrector method is $\Delta\xi = 4 \times 10^{-4}$. The computed local skin-friction coefficient, C_f, is shown in Figure 1 as a function of Re_x. The CPU (Central Processing Unit) time spent on this case is 570 seconds. The measured skin-friction coefficients of Dhawan [27], Smith and Walker [28], and Winter and Gaudet [29] are also given in Figure 1 for comparison. It is clear that the computed C_f is in excellent agreement with the experimental data up to $Re_x = 7.0 \times 10^5$. This implies that the solution method is applicable to complex turbulent flows; however, the accuracy of the result starts to deteriorate further downstream. A close examination of the computed results has shown that the accuracy of the computed effective eddy viscosity distribution across the boundary layer starts to degenerate by exhibiting oscillatory characteristics in the inner region somewhere

after $Re_x = 3.0 \times 10^5$; but a short distance downstream from $Re_x = 3.0 \times 10^5$ the wiggle occurring in the effective eddy viscosity has negligible effect upon the curvature of the solution profile at the boundary, $w_0'(\xi)$, which is linearly proportional to C_f in this case. Figure 2 presents the distribution of the effective eddy viscosity, $\frac{\nu_e}{\nu}$, computed at a number of streamwise stations. The deterioration of the local skin-friction coefficient may be caused by the erroneous distribution of the effective eddy viscosity which may be resulting from the distorted solution profiles obtained in the problem. It is hard to recognize if this is so at this moment.

To gain further insight onto the accuracy and efficiency of the solution technique, the following refined finite element model was considered:

case II: H = 7.0, N = 16, h_i = /3*0.1, 2*0.2, 3*0.3, 0.4, 4*0.5, 3*1.0/.

The numerical integration of the reduced initial value problem is started at $Re_x = 6 \times 10^5$ with the initial profile obtained by interpolating the results of case I. The integration step of Hamming's method with the same accuracy as case I is about $\Delta\xi = 2 \times 10^{-4}$ which is only half of the step size allowed in case I. This reflects the increase in the stiffness of the reduced system of ordinary differential equations due to small element sizes used near the wall; consequently, the efficiency of the method is reduced. The computation for this case was stopped at $Re_x = 10^6$. The computed C_f is also shown in Figure 1 and is quite accurate. The computed effective eddy viscosity distributions also exhibit some oscillatory behavior in the inner region; however, the amplitude of the oscillation is smaller than that in case I at the same

local Reynolds number. This means that the small element sizes used near the wall may have some influence on the computed viscosity distribution. The CPU time used in this case is 200 seconds.

The numerical results obtained from cases I and II seem to indicate that the given value of H may be too large for the flow region considered. In order to investigate the importance of choosing a proper value of H we have also considered the following model:

case III: $H = 5.0$, $N = 10$, h_i = /2*0.1, 0.2, 0.3, 2*0.4, 0.5, 3*1.0/.

The value of $H = 5.0$ corresponds approximately to the boundary layer thickness at $Re_x = 2 \times 10^6$. Again the initial value problem is started at $Re_x = 6 \times 10^5$ using Hamming's method with the initial profile obtained from the result of case I. The computation for this case is terminated at $Re_x = 2 \times 10^6$ and the CPU time required is about 200 seconds. The computed C_f shown in Figure 1 is apparently very acceptable. Figure 3 presents the distribution of $\frac{\nu_e}{\nu}$ computed at a number of local Reynolds numbers. Again the oscillatory behavior starts to show up after $Re_x = 1.0 \times 10^6$. The efficiency of the method can be improved by a small value of H; consequently, a scheme which starts with small H at relatively small boundary layer thickness and increases automatically with increasing boundary layer thickness would be a most effective way for computing the turbulent flows.

The comparison between the computed local skin-friction coefficient for case I and case III shown in Figure 1 seems to imply that the deterioration of the local skin-friction coefficient in case I might be due to the accumulation of errors, which resulted from the extremely large number of integration steps used. The following finite element model, which is the same as case III, is adopted to find out

whether the accumulation error is pronounced or not:

case IV: H = 5.0, N = 10, h_i = /2*0.1, 0.2, 0.3, 2*0.4, 0.5, 3*1.0/.

The computation for this case is carried out in the region of $4.8 \times 10^4 \leq Re_x \leq 2 \times 10^6$. Equation (7-2) is used as the initial profile. The computed C_f is shown in Figure 4. The local skin-friction coefficient obtained in case III is also shown in Figure 4 for comparison. The difference between cases IV and III in the local skin-friction coefficient within the range of $6 \times 10^5 \leq Re_x \leq 2 \times 10^6$ is insignificant. This implies that the accumulation error is not pronounced. Accordingly, the deterioration of the local skin-friction coefficient and the wiggle occurring in the computed effective eddy viscosity may result from other sources. The CPU time used in this case is about 400 seconds.

The numerical results obtained from case IV show that the solution method is indeed applicable to complex turbulent flows and the computed local skin-friction coefficient is in excellent agreement with the experimental data up to a local Reynolds number of $Re_x = 2 \times 10^6$. However, the solution method is not efficient because of the small integration step required. This motivated the investigation on integration methods to overcome the numerical instability. The numerical results obtained by Hamming's method indicated that the reduced equations are stiff due to the fact that the average integration step size required is much smaller than that needed by the solution behavior. Gear's method for stiff equations is chosen to efficiently solve the reduced initial value problem. The DIFSUB subroutine subprogram (Gear, [30]) of Gear's method has been modified and incorporated into the main program to solve the reduced initial problem. The accuracy of the method is

assigned as 10^{-4}. Moreover, since the boundary layer thickness of turbulent flows increases with ξ and its growth rate is hard to foresee, it is generally impractical to select a large constant value of H for the flow region considered. Therefore, the program is also implemented to automatically adjust the boundary layer thickness, H, based on an empirical formula. In this study the boundary layer thickness is assumed to be 8.5 times the displacement boundary layer thickness. The number of elements is increased in the program to account for the growth of the boundary layer. The maximum allowable integration step is limited to 10^{-2} in DIFSUB subroutine.

The following finite element model was used to start the intital value problem for demonstrating the efficiency of Gear's method:

case V: H = 4.0, N = 8, h_i = /2*0.1, 0.3, 3*0.5, 2*0.1/ .

The computation is started right after the transitional point at $Re_x = 6.0 \times 10^4$ with the initial condition given by equation (7-2) and is carried out up to $Re_x = 2.24 \times 10^6$. The final boundary layer thickness and the number of elements are H = 6 and N = 10, respectively. The CPU time spent on this case is only 22 seconds, which is approximately 20 times less than that required for case IV. It is clear that the efficiency of the solution method has been drastically improved by using Gear's method. Moreover, the computed results showed that the deterioration of the effective eddy viscosity starts somewhere after $Re_x = 1.1 \times 10^6$ and the wiggle in the effective eddy viscosity occurs in the neighborhood of $\eta = 1.0$ in this case; on the contrary, the deterioration and wiggle of the effective eddy viscosity occurs after $Re_x = 1.5 \times 10^6$ and $\eta = 0.7$, respectively, in case IV. When comparing the element size distribution

in case IV and case V, one may tell that the deterioration of the effective eddy viscosity takes place at different local Reynolds number and the wiggle in the computed effective eddy viscosity occurring at different locations in the η direction may be due to the erroneous solution profiles which result from truncation errors. This fact seems to imply that the effective eddy viscosity can be very sensitive to the solution profiles.

Since the stiffness problem induced by using the small element sizes near the wall has been overcome by using Gear's method for stiff equations, how the effective eddy viscosity is influenced by very small elements near the wall can be investigated numerically. The finite element model case VI was arranged for this purpose:

case VI: H = 4.0, N = 9, h_i = /2*0.05, 0.1, 0.3, 3*0.5, 2*1.0/.

The computation covers the region of $6.0 \times 10^4 \leq Re_x \leq 2.57 \times 10^6$. Deterioration of the effective eddy viscosity takes place further downstream after $Re_x = 2.1 \times 10^6$, and the wiggle which occurs in the computed effective eddy viscosity is still in the neighborhood of $\eta = 1.0$. These results show that the very small element sizes used near the wall can defer the occurrence of the deterioration of the effective eddy viscosity.

The next problem one needs to investigate is whether or not the element sizes not in the immediate vicinity of the wall have any influence on the calculation of the effective eddy viscosity. The following finite element model was designed for this purpose:

case VII: H = 5.0, N = 11, h_i = /2*0.05, 0.1, 0.2, 2*0.3, 2*0.5, 3*1.0/.

The element sizes are slightly changed within the range of η = 0.0 to η = 1.0 compared with case VI. The computation for the reduced initial value problem is started at $Re_x = 2.0 \times 10^6$ and proceeds to $Re_x = 1.47 \times 10^7$. The deterioration of the effective eddy viscosity still occurs; however, the wiggle in the effective eddy viscosity is shifted farther from the wall in the neighborhood of η = 1.50 instead of η = 1.0 in case VI.

Since in cases VI and VII we found that small elements near the wall can defer the occurrence of the deterioration of the effective eddy viscosity, and small elements used not in the immediate vicinity of the wall can shift the location of the wiggle farther away from the wall, it is believed that a slight variation of the solution characteristics can very significantly affect an accurate calculation of the effective eddy viscosity. In order to gain further insight the variation of the solution $w(\xi, \eta)$, its first derivative at η_1 and second derivative at η_0 obtained from case VI are shown as functions of Re_x in Figures 5 and 6. Upon close examination of the results in these figures, it is evident that the first element size smaller than 0.05 should be used if the computation proceeds to local Reynolds number greater than 10^6.

Most of the finite difference methods available for turbulent flows have been tested only for the region in which the local Reynolds number is less than 2×10^6. However, in this study we are especially interested in applying the finite element-differential method to sufficiently high local Reynolds number in order to find some information on the flow characteristics.

The Gauss-Legendre quadrature formula worked very well in the laminar region (i.e. $\frac{\nu_e}{\nu} = 1$) and its applicability in the turbulent region is expected to be good as well. However, due to the two-layer eddy viscosity model, in which the slope of the eddy viscosity is discontinuous at the matching point which separates the inner and outer regions, the Gauss-Legendre quadrature may not be suitable for direct evaluation of the integral over the element which contains the matching point. When the local Reynolds number is not high, the term involving the discontinuous slope of the effective eddy viscosity is much smaller than other terms on the right hand side in equation (3-30). The errors involving the integral in using the Gauss-Legendre quadrature on the discontinuous function may not be significant. However, when the local Reynolds number reaches a certain number, the magnitude of the discontinuous function is pronounced. The errors introduced by this inaccurate approximation of the integral involving the discontinuous function result in a very small integration step in which the assigned computer time is used up. The termination of the computation in case VI resulted from this improper integration. Hence, a special measure is required for the evaluation of the integral involving a discontinuous function. For instance, the integral can be divided into two parts and then Simpson's rule can be used for the evaluation.

In the process of computation the matching point has to be determined at each streamwise station. The following scheme was used to find the matching point. First each element is further divided into 10 equal subintervals. The effective eddy viscosity is computed from the wall outward at each joint node of the subintervals and compared with that in the outer region. If at a certain joint node the effective eddy viscosity is larger than that in the outer region, the effective eddy

viscosity is then computed at a location which is less than the previous location by half the previous increment. If the newly computed effective eddy viscosity is less than that in the outer region, the effective eddy viscosity is again computed at a new location which is larger than the previous location by half the increment. This procedure is repeated until enough points in the inner region are generated. Finally, the matching point is obtained by extrapolation using a polynomial of degree two. After the matching point is determined, Simpson's rule can be applied to evaluate the integral over the special element in which the integrand is a discontinuous function.

The next numerical experiment was to investigate the accuracy of the algorithm for determining the matching point. The finite element model employed to start the initial value problem, equation (5-8) and equation (7-2), is

case VIII: $H = 3.5$, $N = 11$, h_i = /2*0.05, 0.1, 0.2, 2*0.3, 5*0.5/.

The initial condition is applied at $Re_x = 5.5 \times 10^4$ and the integration routine employed is the newly acquired subroutine package LSODE which is the latest version of the Gear method developed at Lawrence Livermore Laboratory. The computed matching point shows irrational behavior after $Re_x = 1.52 \times 10^6$. This results in a small integration step and the computation hardly proceeds downstream. The typical jumping characteristics of the computed matching points are given in Figure 7. Since the matching point represents the growth of the inner region, it should be monotonically increasing as the computation proceeds downstream. The incorrectly determined matching point may be due to improper extrapolation or other causes.

If the incorrectly determined matching point is due to improper extrapolation, the difficulty can be overcome by modifying the original algorithm for finding the matching point. The modified algorithm is that one of the extrapolation points would be close enough to the effective eddy viscosity in the outer region by the difference of).5 when the effective eddy viscosity in the outer region is greater than 50. If the computed eddy viscosity is less than 50 the original scheme is used.

Another numerical experiment was conducted and the result obtained indicated that the alternate jumping characteristics of the determined matching points is not due to inaccurate extrapolation but due to the wiggle in the computed effective eddy viscosity. The wiggle can result in difficulty in finding the matching point at high local Reynolds number, which is important to the solution method.

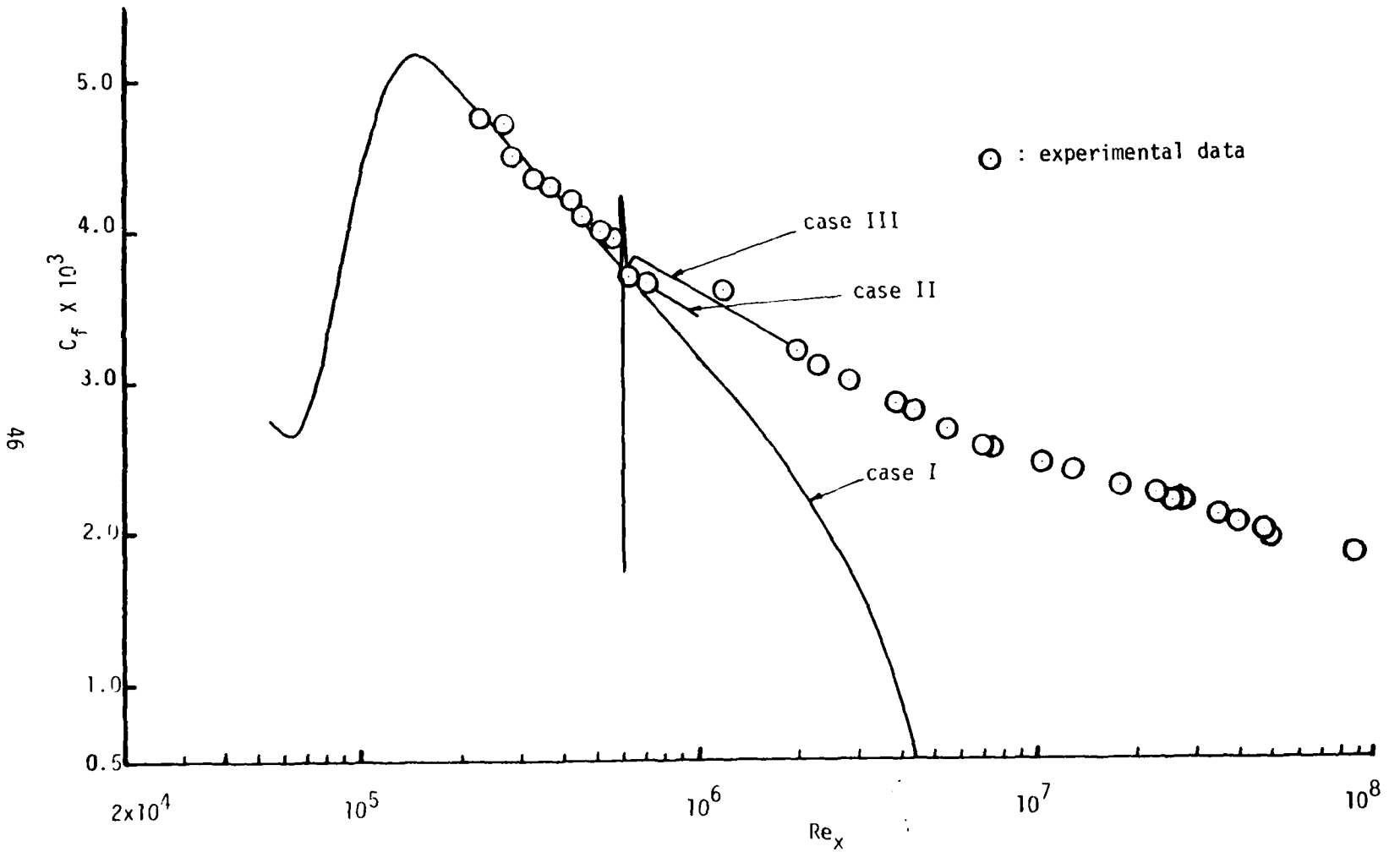

Figure 1. Computed local skin-friction coefficients for turbulent flow over a flat plate.

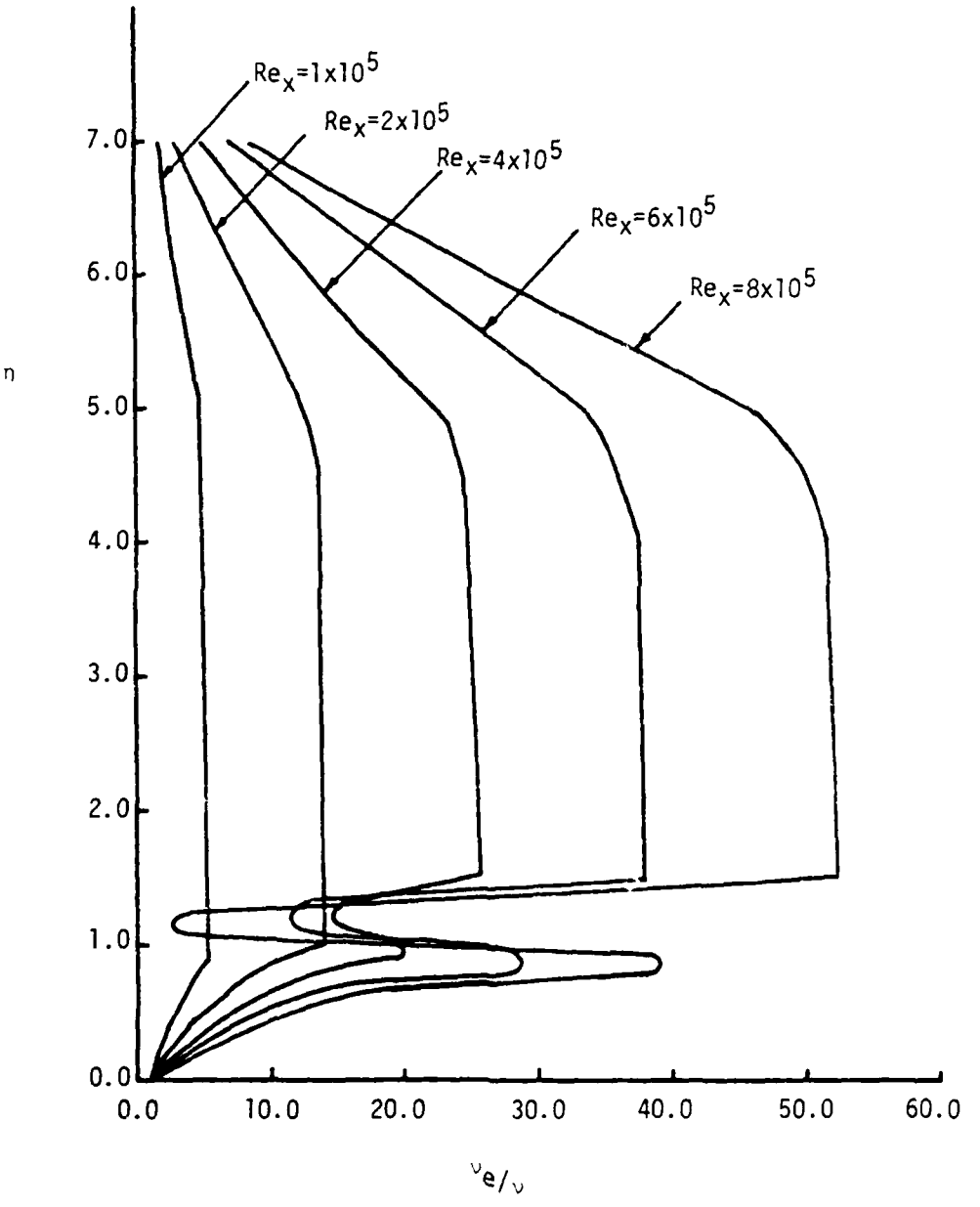

Figure 2. Computed effective eddy viscosity distribution from case I at different local Reynolds numbers.

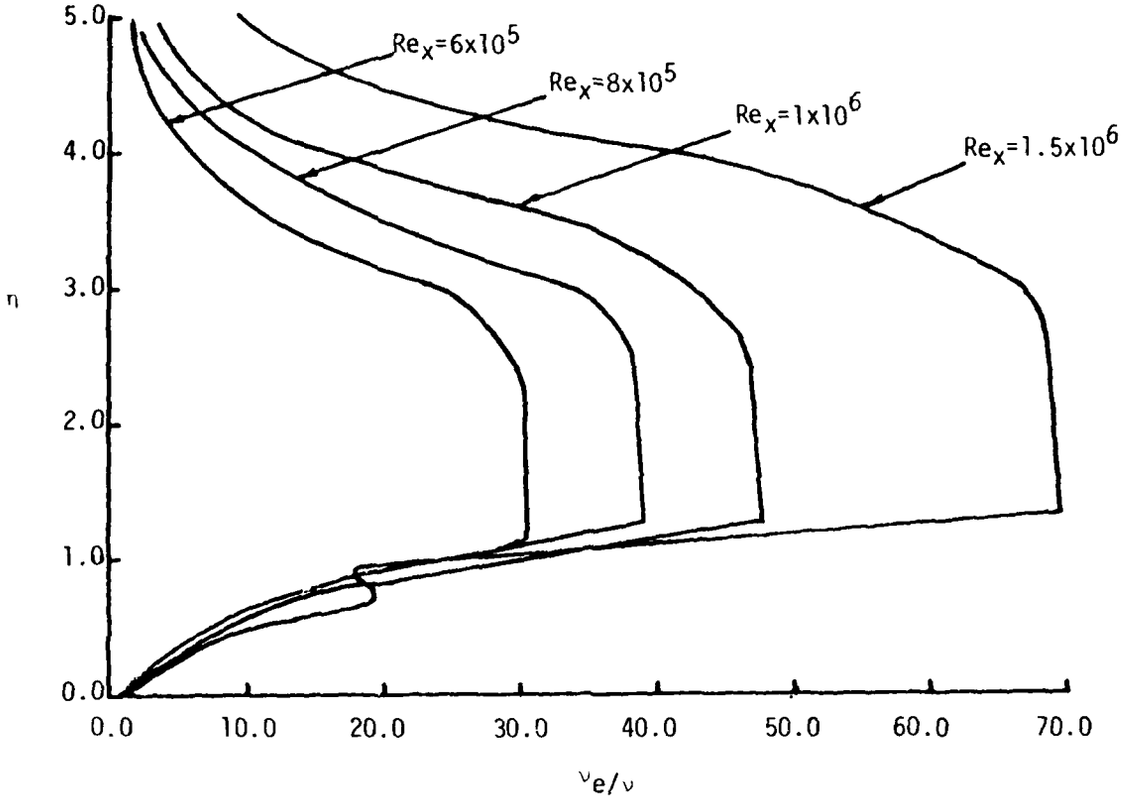

Figure 3. Computed effective eddy viscosity distribution from case III at different local Reynolds numbers.

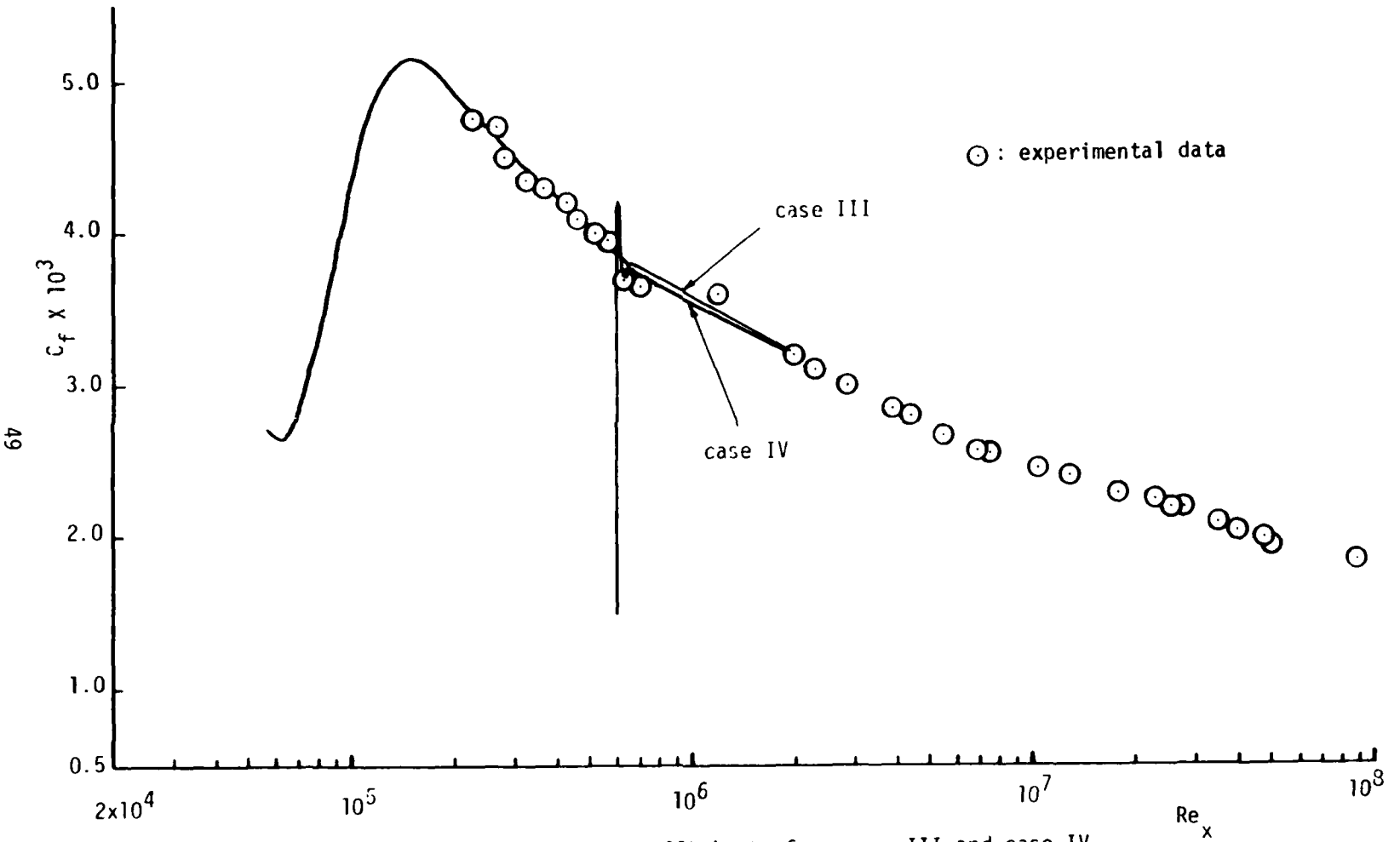

Figure 4. Computed local skin-friction coefficients from case III and case IV.

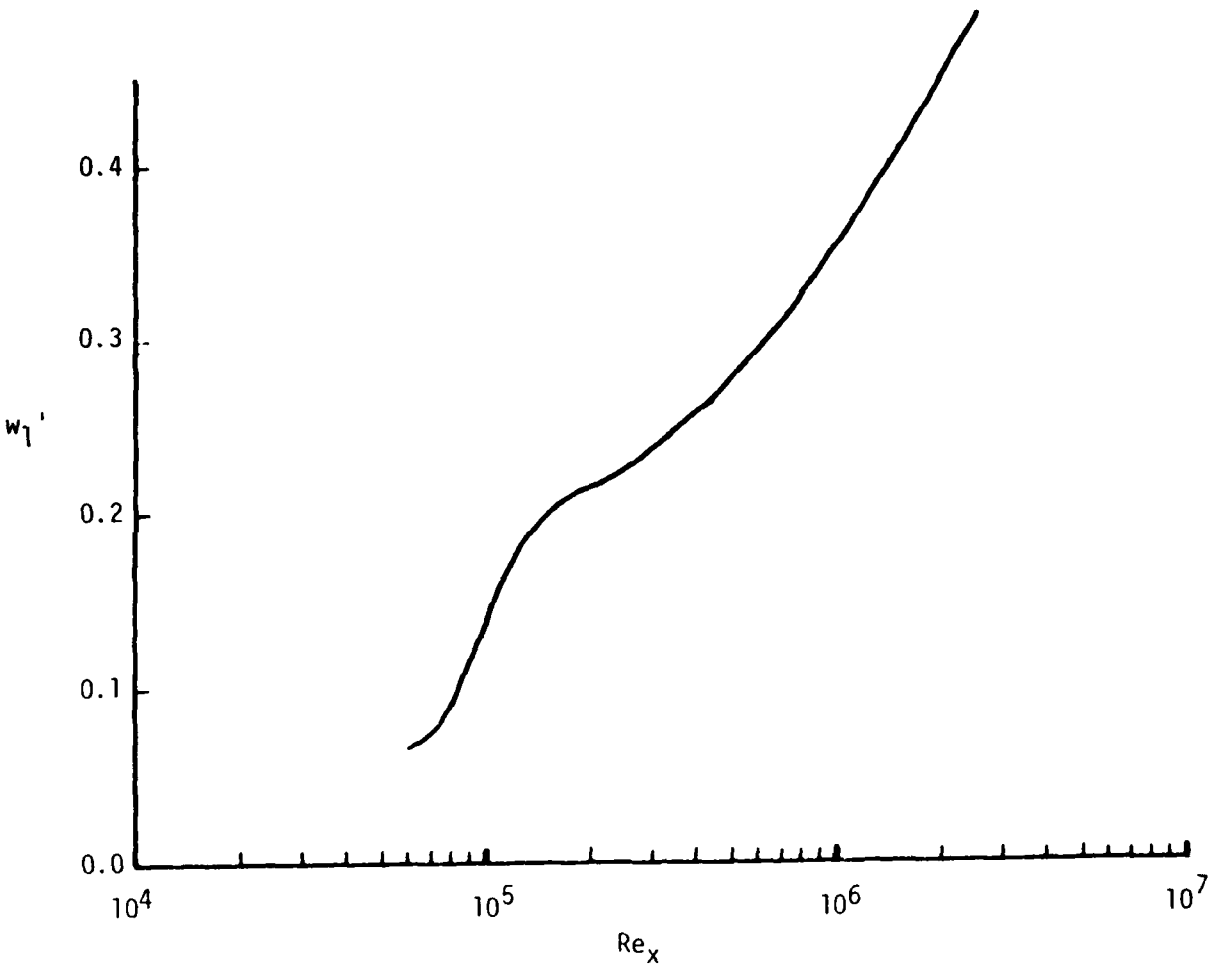

Figure 5. First derivative of solution profile with respect to η at $\eta=0.05$ from case VI.

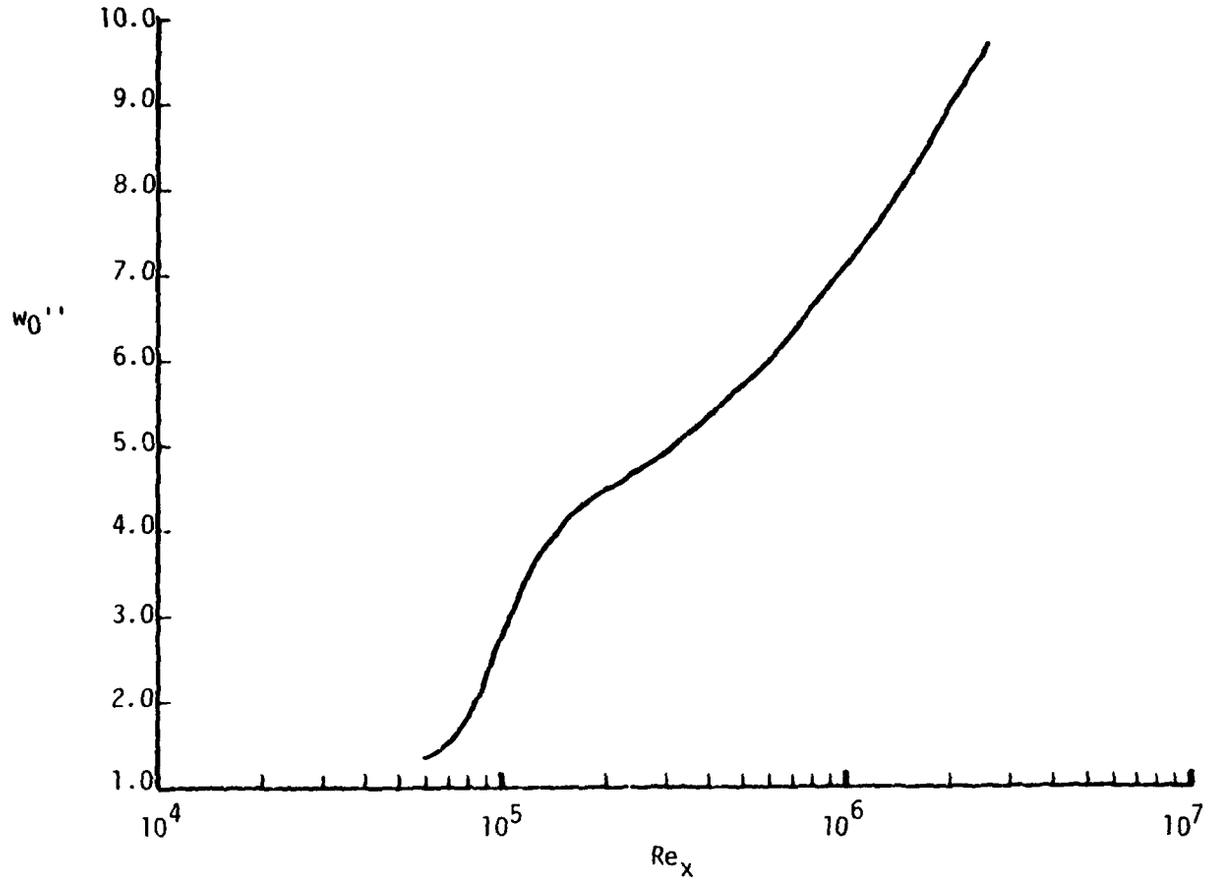

Figure 6. Second derivative of solution profile with respect to η at η=0.0 from case VI.

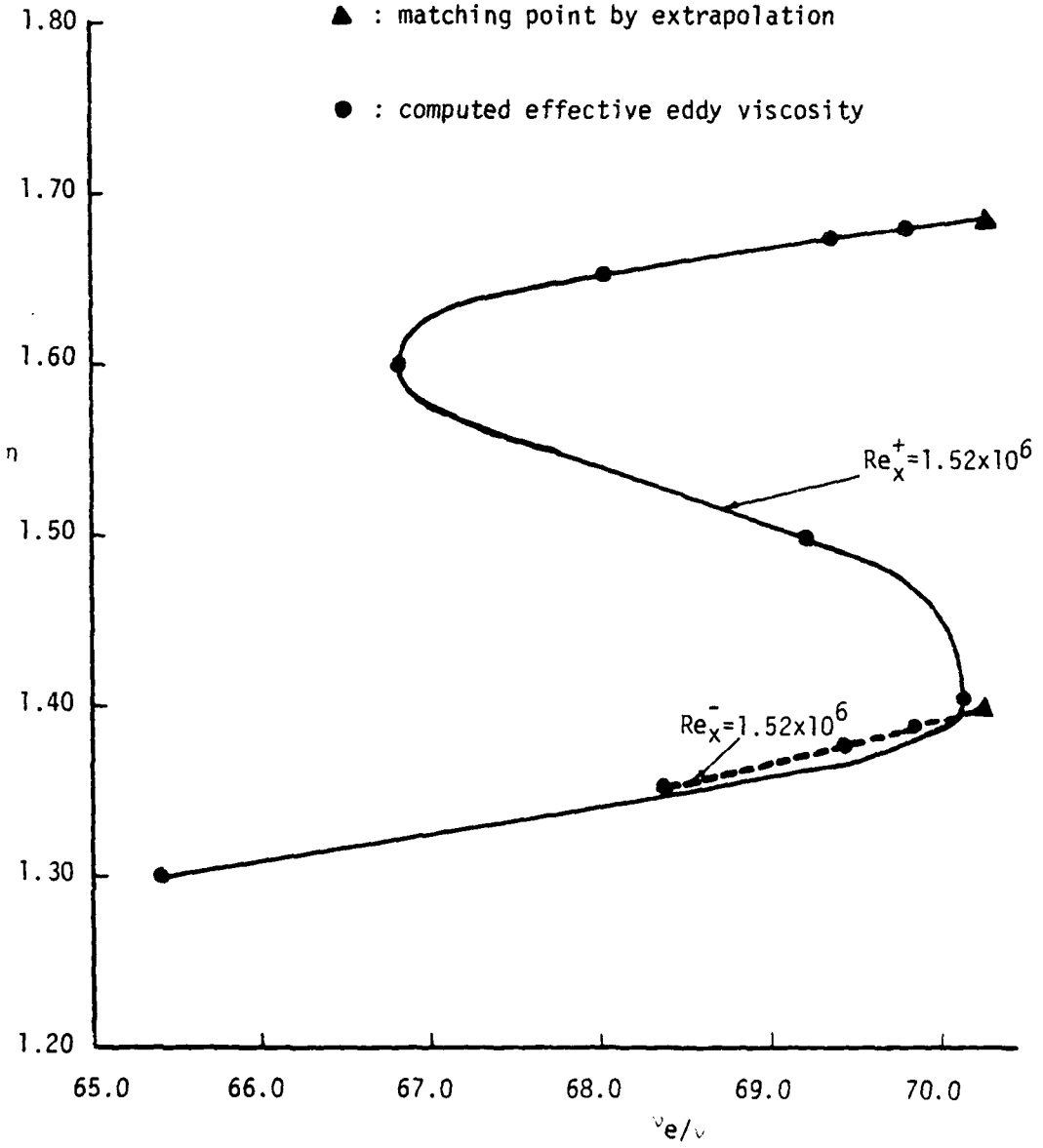

Figure 7. Jumping of matching point in the vicinity of $Re_x=1.52x10^6$ from case VIII:--------,$Re_x=1.52193x10^6$; ————, $Re_x=1.52196x10^6$.

CHAPTER VIII
RESULTS AND DISCUSSION

The preliminary numerical experiments show that the choice of the first element size h_1 and other element sizes in the inner region can be decisive in the computation of turbulent flows. The improper discretization of the flow region can result in inaccurate solution profiles which deteriorate the accuracy of the effective eddy viscosity. The wiggle occurring in the effective eddy viscosity distribution across the boundary layer can result in difficulties in finding the matching point, which is very important to the solution method. Moreover, the properly chosen value of H can be crucial to the accuracy of the solution as well as to the efficiency of the method. The stiffness problem of the reduced equations has been overcome by using Gear's method.

According to the findings in case VI, the small first element size less than 0.05 seems to be needed for computations which proceed to high local Reynolds number. The following two finite element models are designed to find how the solution is affected by the small first element size as well as the element sizes in the inner region at high Reynolds numbers:

case IX: H = 6.5, N = 18, h_i = /2*0.02, 2*0.03, 2*0.05, 0.2, 7*0.3, 2*0.5, 1.0, 2.0/

case X: H = 6.5, N = 16, h_i = /2*0.02, 2*0.03, 2*0.05, 0.2, 2*0.3, 5*0.5, 1.0, 2.0/.

The first element size used in both cases is 0.02. The difference between these two models is only in the element sizes near the matching point but still in the inner region. The integration of the initial value problem for case IX and case X is started at $Re_x = 2.2 \times 10^6$ and 1.1×10^6, respectively. The computed local skin-friction coefficients in Figure 8 compare satisfactorily with the measured data. The computed effective eddy viscosity is therefore found to be correct. No wiggle occurs in the effective eddy viscosity distribution in either case in the course of integration up to $Re_x = 1.0 \times 10^7$. This indicates that the wiggle which deteriorates the effective eddy viscosity distribution can be due to the large first element size. The relatively large element sizes away from the boundary may not be critical to the solution.

For the high local Reynolds number, the solution profiles change very rapidly in the vicinity of the wall. The small first element size is absolutely necessary to take care the variation of the solution profile there. So far we know that the first element size 0.02 gives good results up to $Re_x = 1.0 \times 10^7$; we would like to know whether this first element size 0.02 is still valid further downstream. The finite element model for this purpose was given by

case XI: H = 4.0, N = 15, h_i = /2*0.02, 2*0.03, 2*0.05, 0.2, 2*0.3, 6*0.5/.

The initial condition, equation (7-2), is employed to start the initial value problem at $Re_x = 5.47 \times 10^4$. The growth of the boundary layer thickness is automatically adjusted by the empirical formula. Whenever the boundary layer thickness (H) changes, the increment is $\Delta H = 1$. The number of elements is increased by two; each has the element size 0.5.

The computed local skin-friction coefficient shown in Figure 9 is in excellent agreement with the experimental data up to $Re_x = 5.0 \times 10^7$. The deterioration of the effective eddy viscosity again takes place somewhere after $Re_x = 2.0 \times 10^7$. The computation is terminated at $Re_x = 8.6 \times 10^7$ with H = 12 and N = 31. The CPU time spent on this case is 250 seconds. The matching point as a function of Re_x, given in Figure 10, shows the growth of the inner layer. The matching point after 3×10^7 starts to decrease as the local Reynolds number increases. These results reflect that the solution profile can be affected by the wiggle in the effective eddy viscosity after $Re_x = 3 \times 10^7$. The computed displacement boundary layer thickness grows very fast as the local Reynolds number increases. Consequently, a special measure in choosing the value of H is needed for sufficiently high local Reynolds number. The curvature w_0'' and the first derivative w_0' are also given in Figures 12 and 13, respectively. Both w_0'' and w_1' deteriorate near the trailing edge of the curves. This suggests that a very small first element size, less than 0.02, must be used further downstream.

Since the accuracy of the solution profile is mostly determined by the first element size, the first element size obtained by cutting $h_i = 0.02$ of case XI in half is used in the following finite element model to investigate how the accuracy of the solution improved:

case XII: H = 4.0, N = 16, h_i = /2*0.01, 0.02, 2*0.03, 2*0.05, 0.2, 2*0.3, 6*0.5/.

The initial value problem is solved in the region $8.1 \times 10^3 \leq Re_x \leq 7.8 \times 10^7$. The computed skin-friction coefficient in Figure 14 is

indeed improved and is good up to 7.8×10^7. It is clear that the small first element size is certainly needed for accurate prediction of the local skin-friction coefficient. The computed effective eddy viscosity without using transverse intermittency at several local Reynolds numbers are given in Figures 15, 16, 17 and 18, respectively. The dotted lines in Figures 15, 16, 17 and 18 represent the effective eddy viscosity computed by the inner region formulation above the matching point. The solid lines represent the effective eddy viscosity distribution across the boundary layer. The computed effective viscosity in Figure 15, 16 and 17 are good but not so in Figure 18. The wiggle occurring in the inner region may not deteriorate the solution until the wiggle is of sufficient magnitude to cause the sign of the first derivative of the effective eddy viscosity with respect to η to alternate. In order to eliminate the wiggle a first element size smaller than 0.01 seems to be required further downstream. The final boundary layer thickness is $H = 12$ with 24 elements. The increment of the boundary layer thickness is $\Delta H = 2$. The corresponding increment of the elements is 2; each has element size 1.0. The total CPU time for this case is 350 seconds.

Because the computation was carried out in the transformed plane, one would like to know what the corresponding physical plane looks like. The relationship between η and y_1 is of major interest. The functional relation obtained from case XI is given in Figure 19. The transformation used to stretch the coordinate y_1 seems to be suitable for the boundary layer flow problems in this study. Consequently, the number of nodal points required for the solution method can be reduced without loss of accuracy. This leads to computational efficiency.

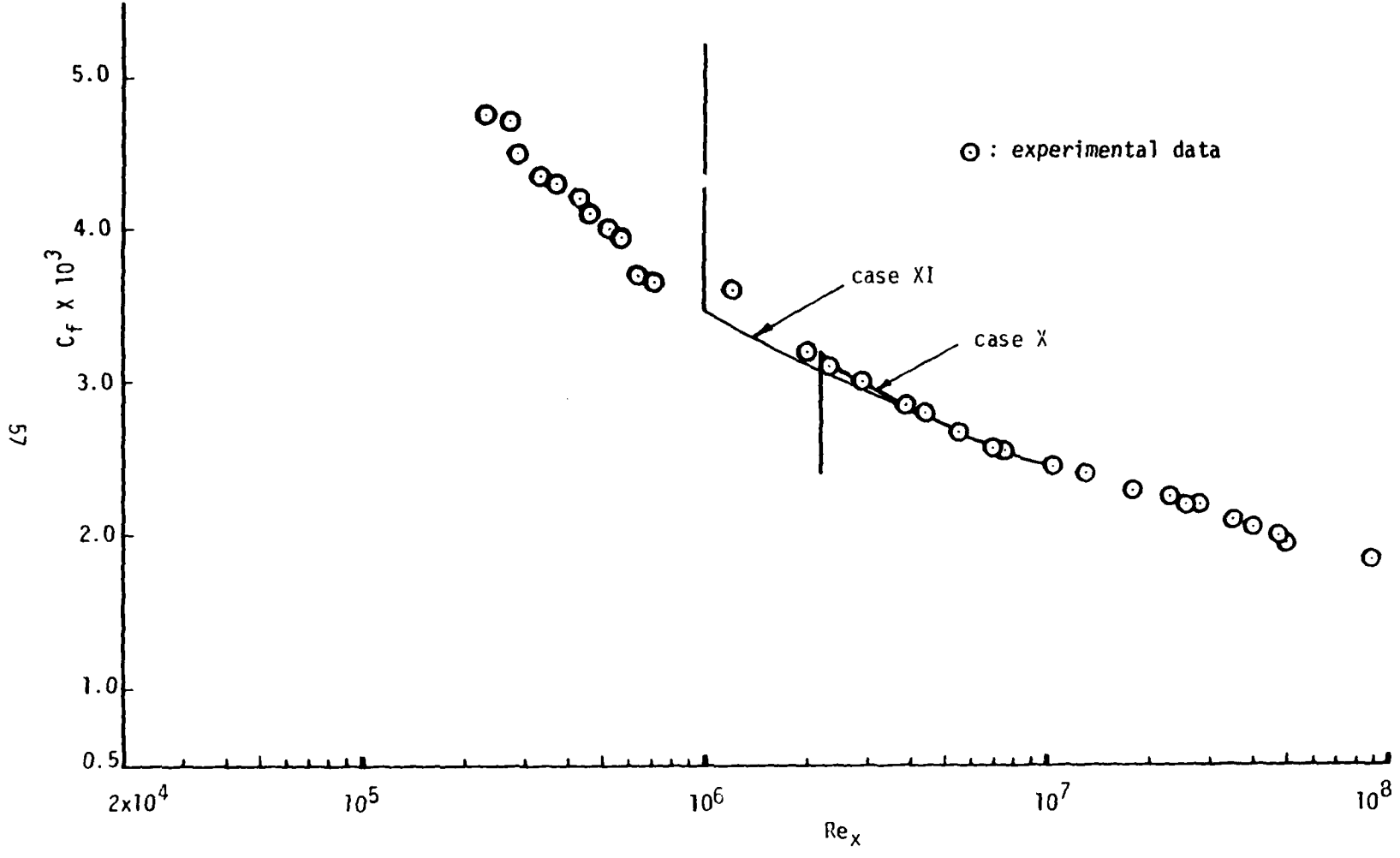

Figure 8. Computed local skin-friction coefficients from case IX and case X.

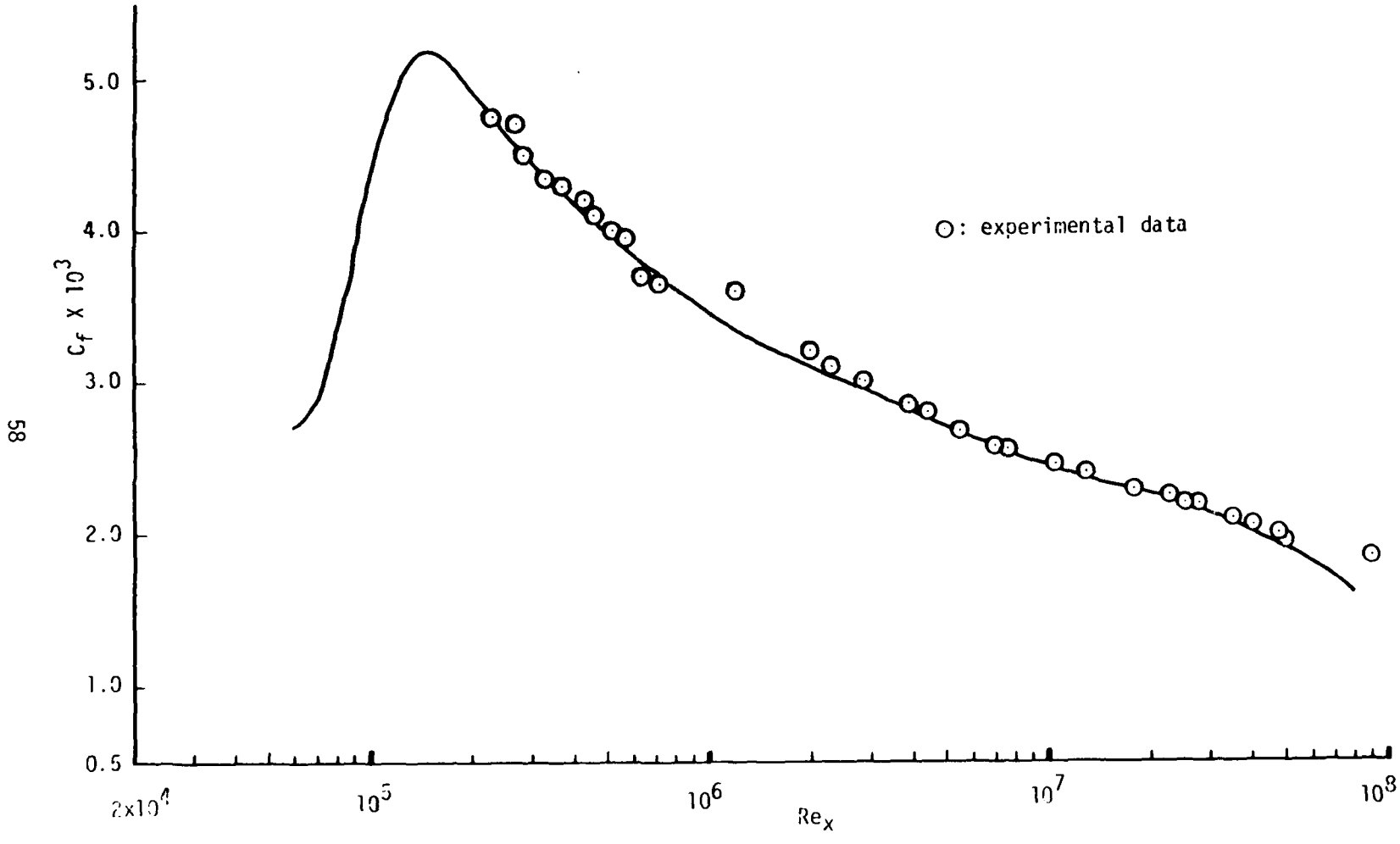

Figure 9. Computed local skin-friction coefficient from case XI.

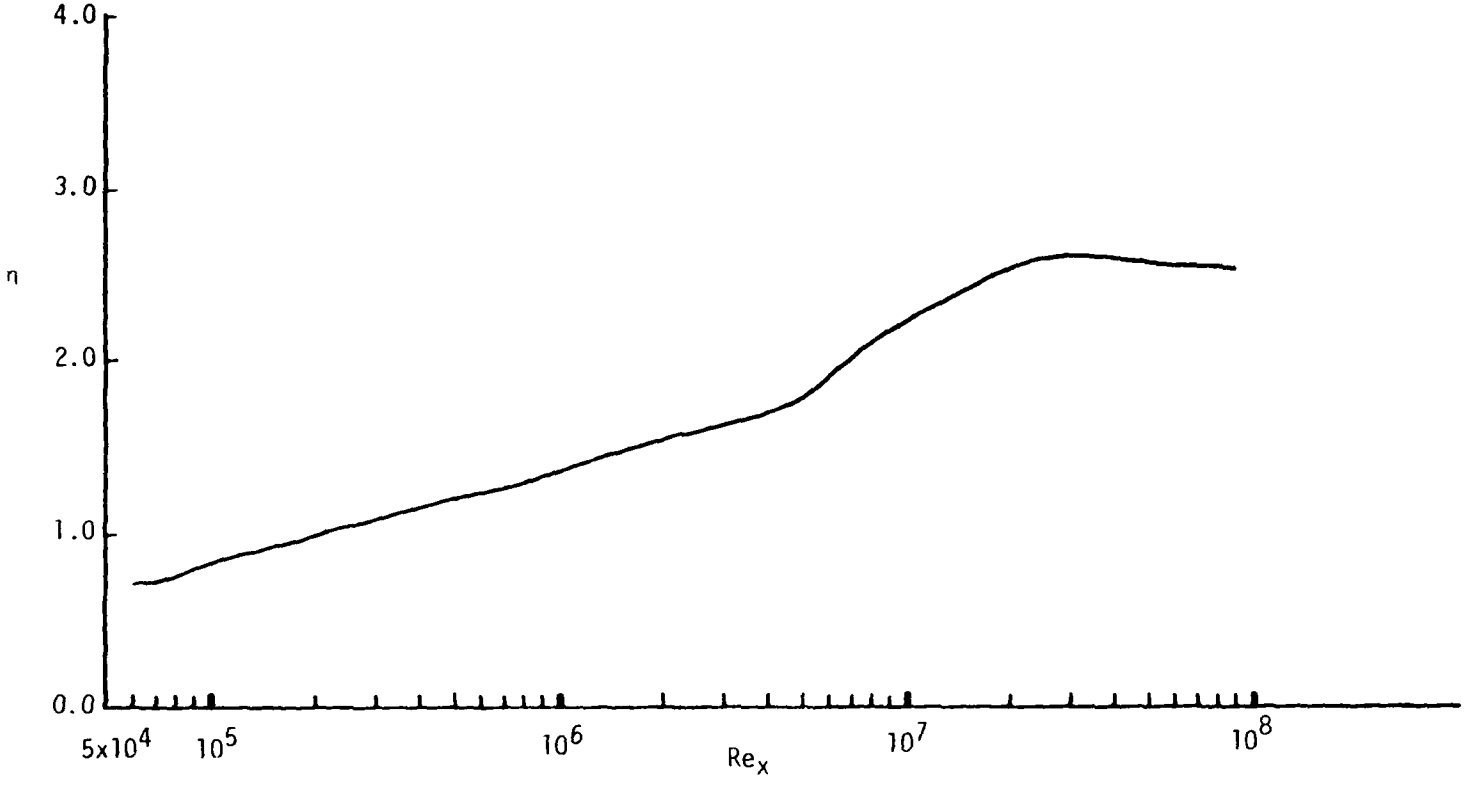

Figure 10. Growth of matching point from case XI.

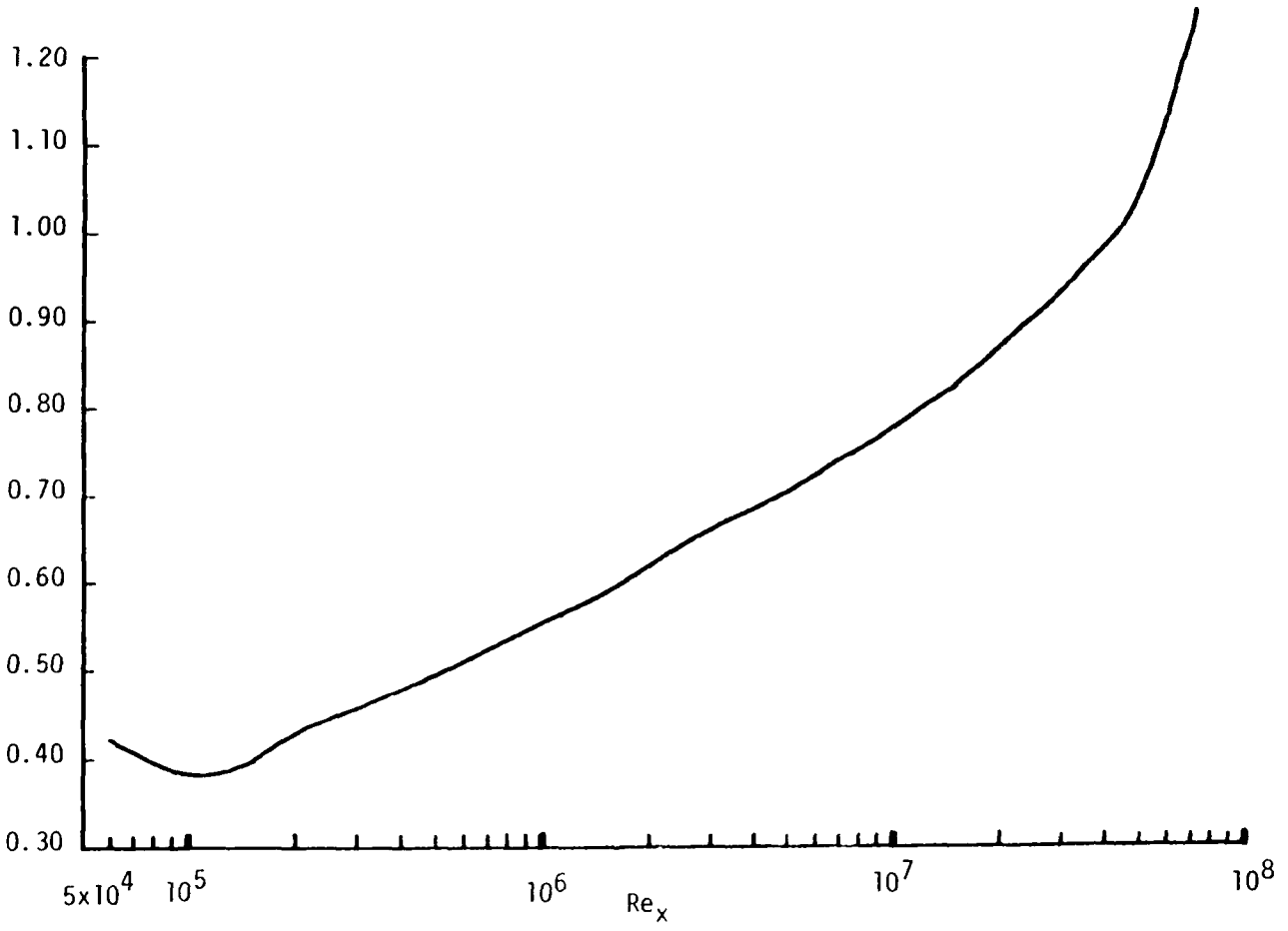

Figure 11. Growth of displacement boundary layer thickness, equation (2-12), from case XI.

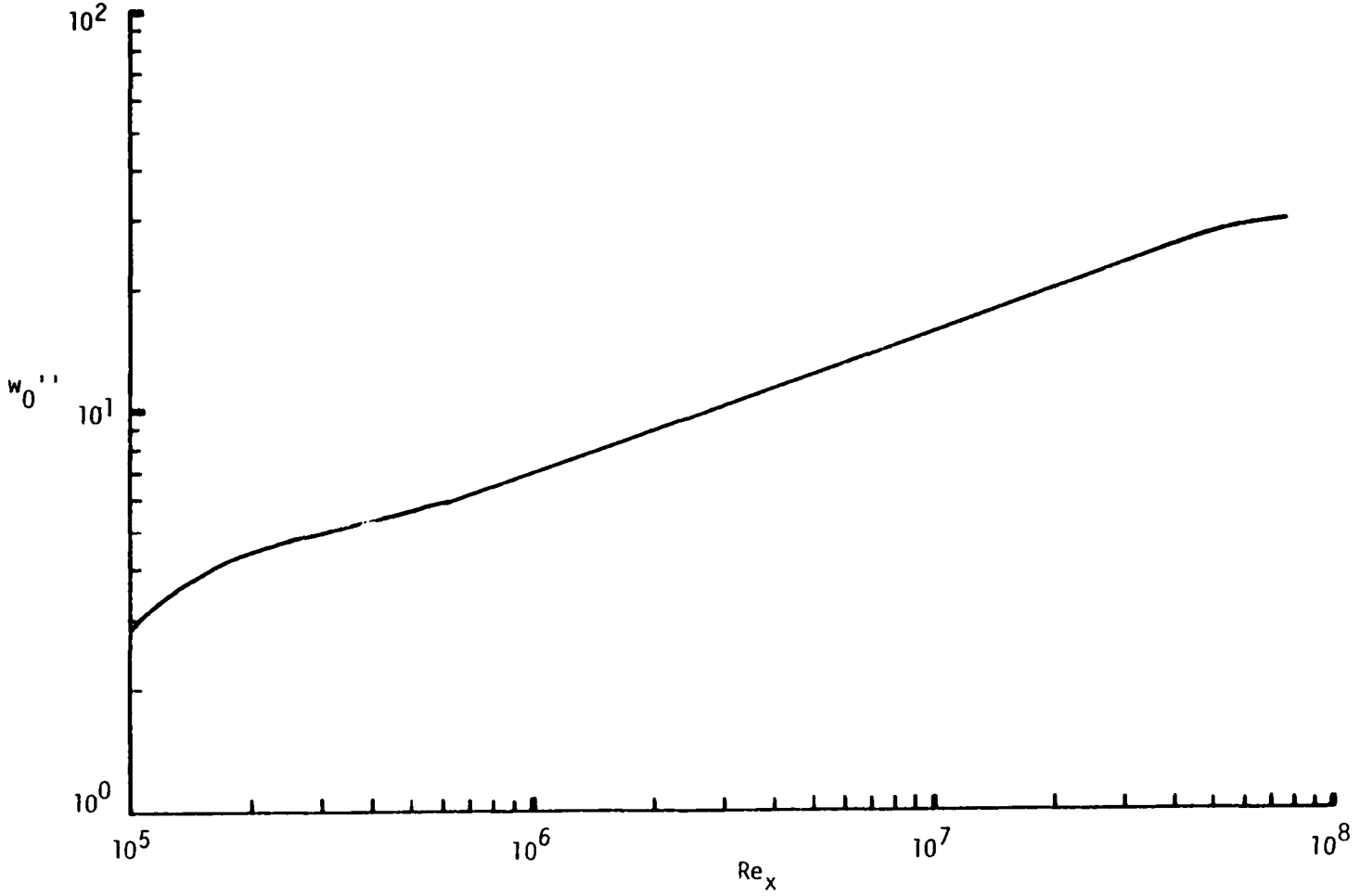

Figure 12. Second derivative of solution profile with respect to η at η=0.0 from case XI.

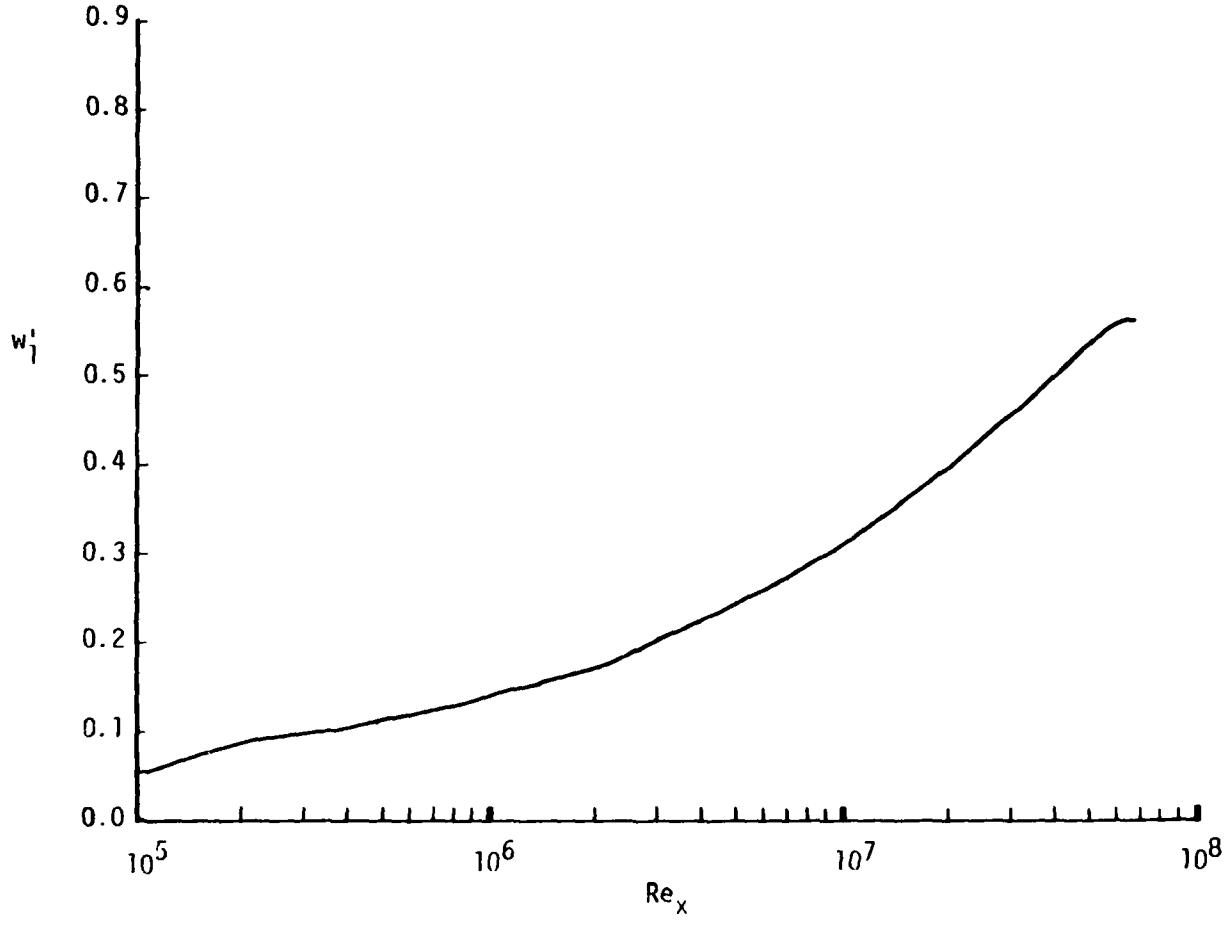

Figure 13. First derivative of solution profile with respect to η at η=0.02 from case XI.

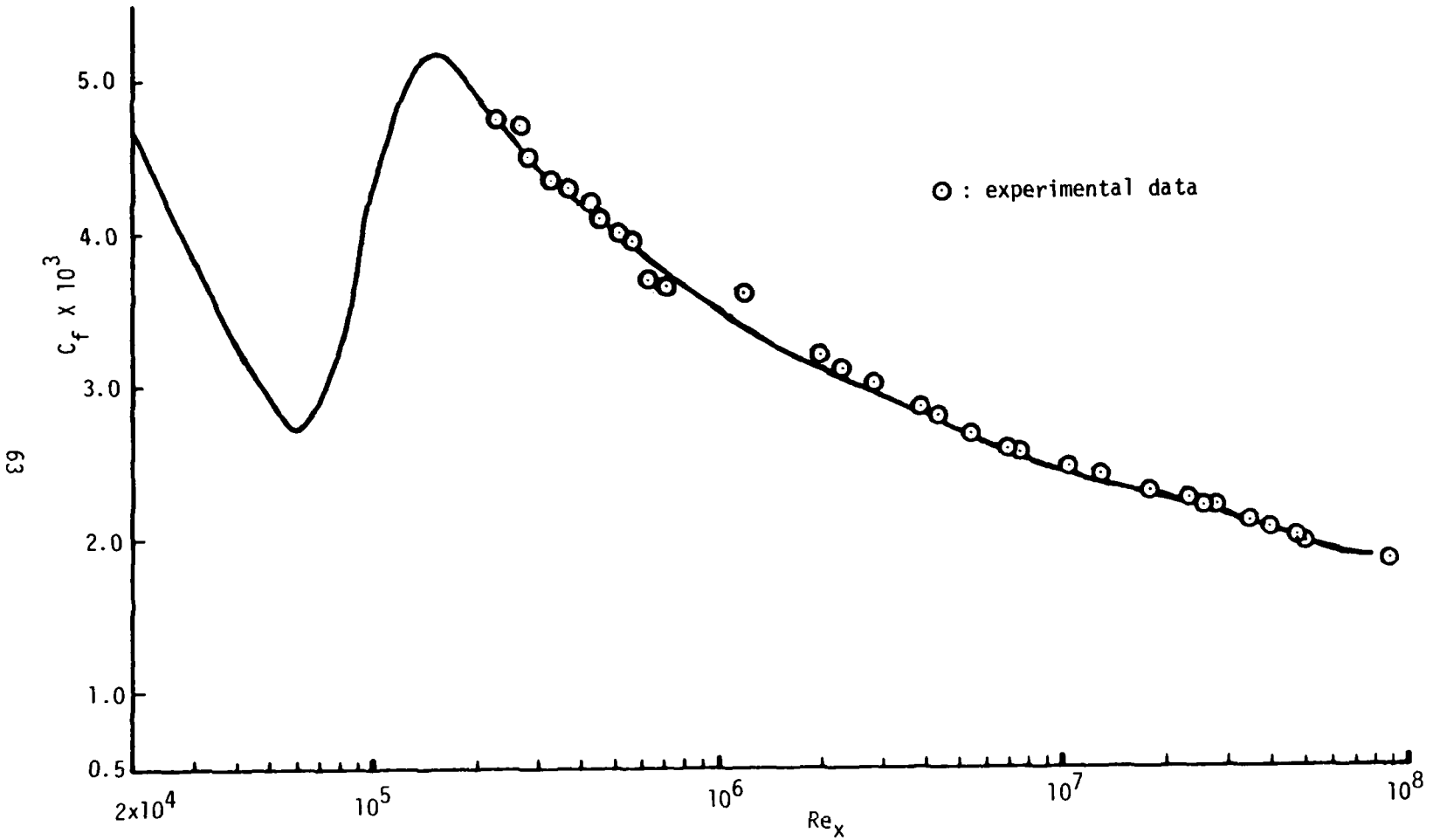

Figure 14. Computed local skin-friction coefficient from case XII.

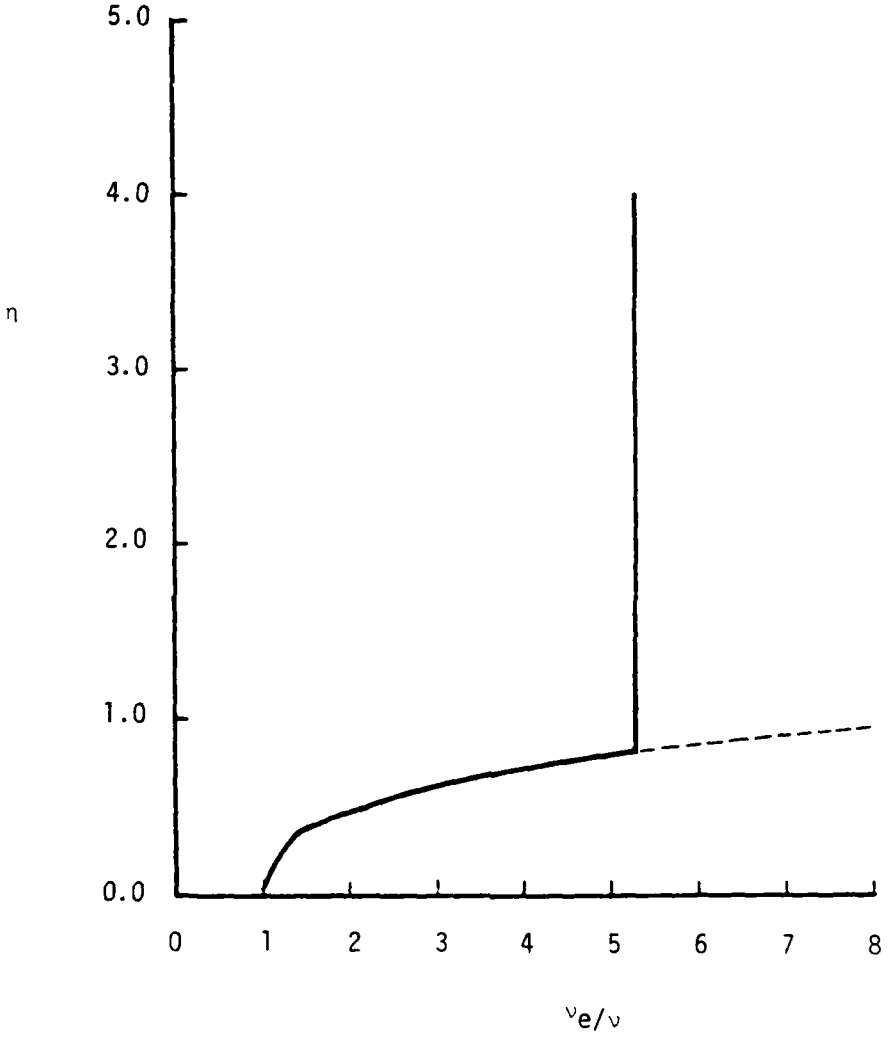

Figure 15. Computed effective eddy viscosity distribution at $Re_x=1x10^5$ from case XII.

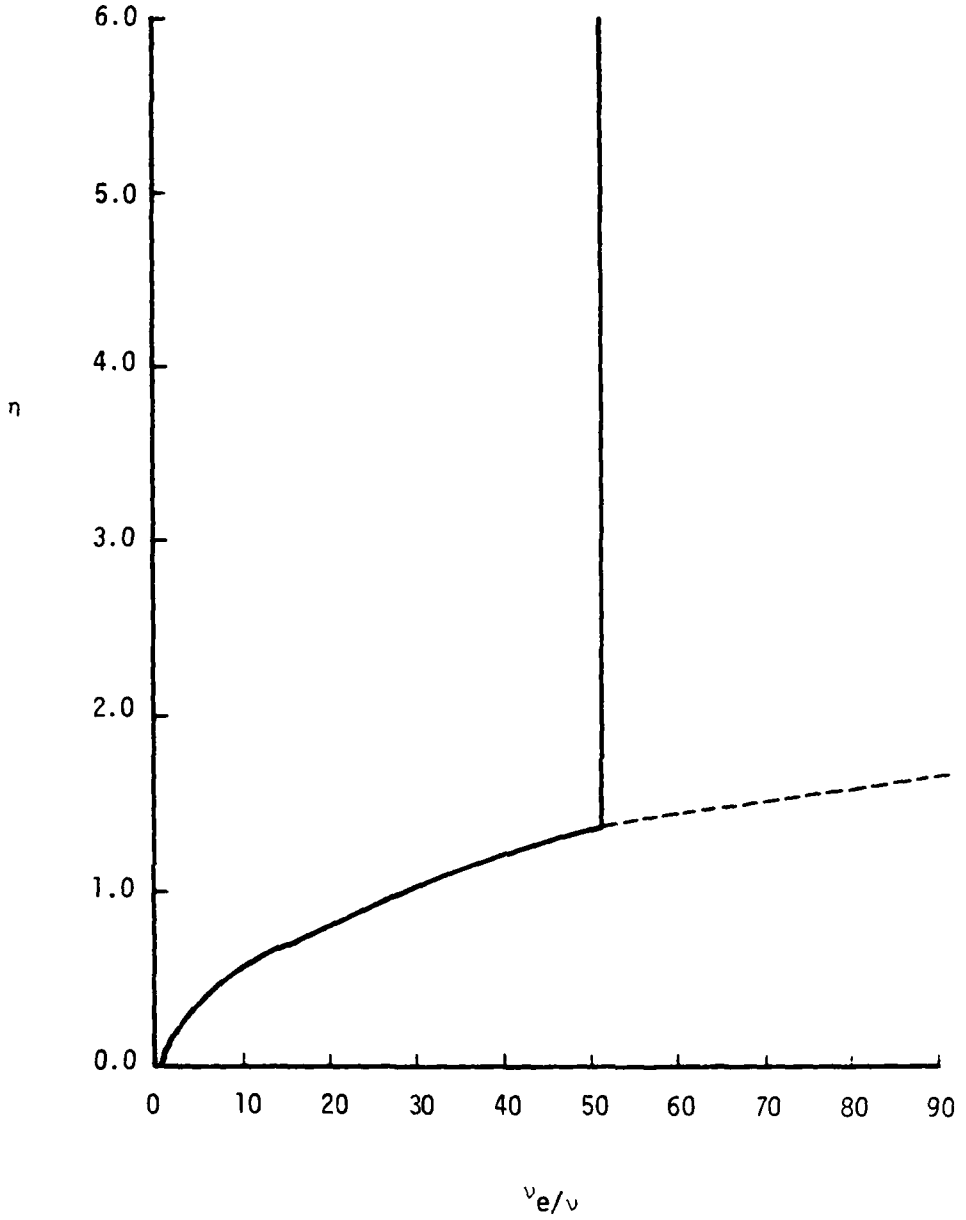

Figure 16. Computed effective eddy viscosity distribution at $Re_x=1x10^6$ from case XII.

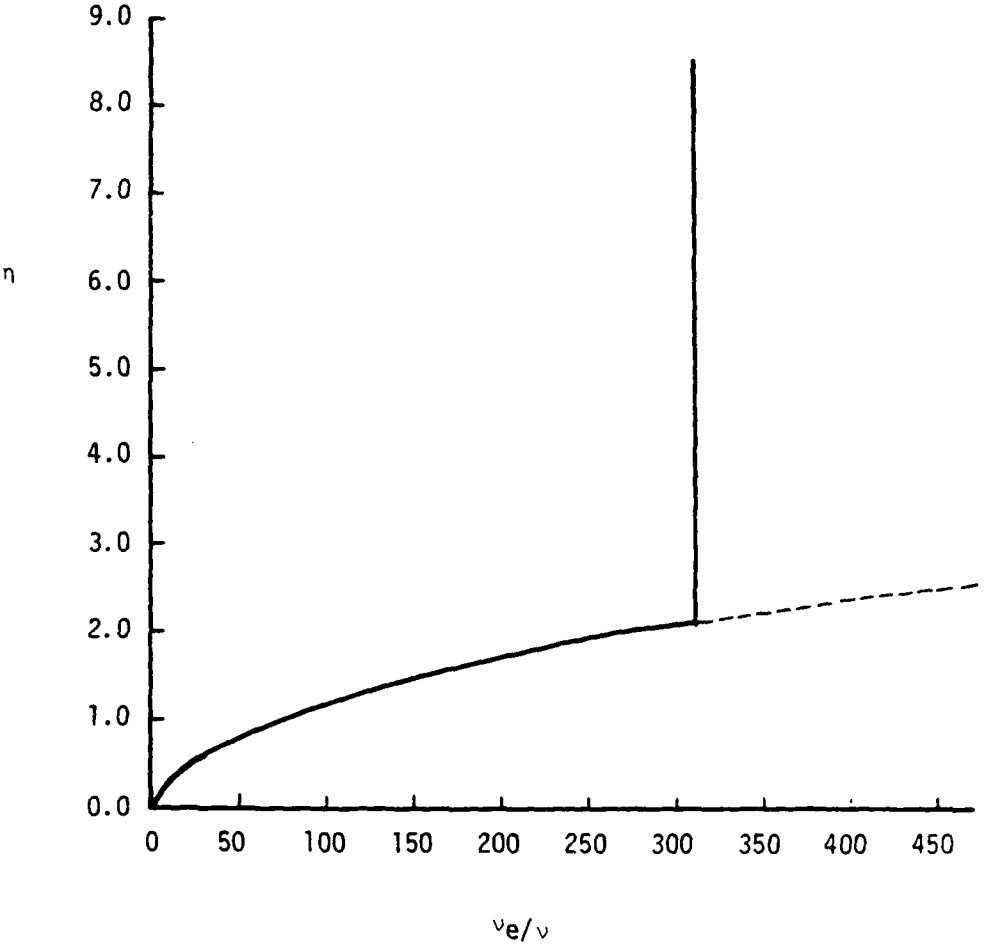

Figure 17. Computed effective eddy viscosity distribution at $Re_x = 1 \times 10^7$ from case XII.

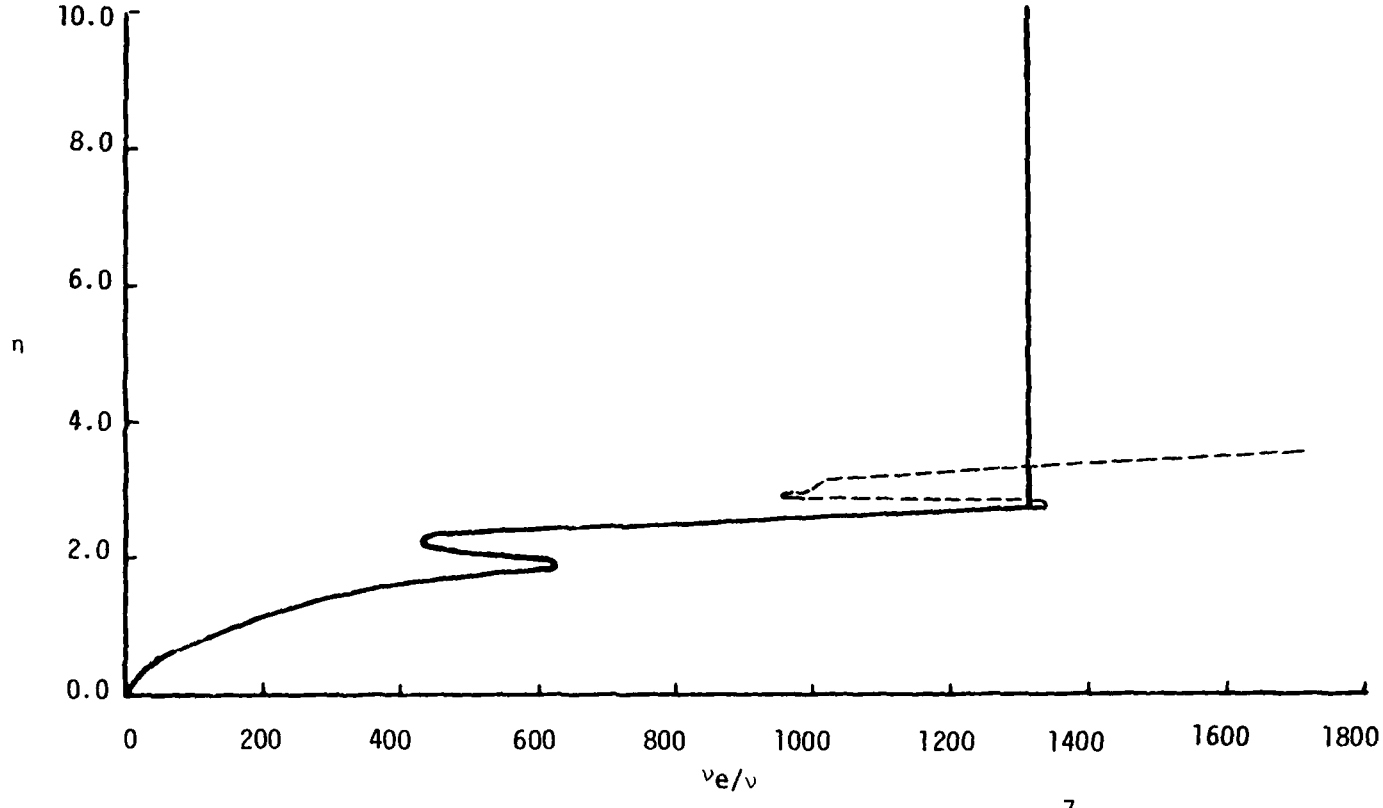

Figure 18. Computed effective eddy viscosity distribution at 5.5×10^7 from case XII.

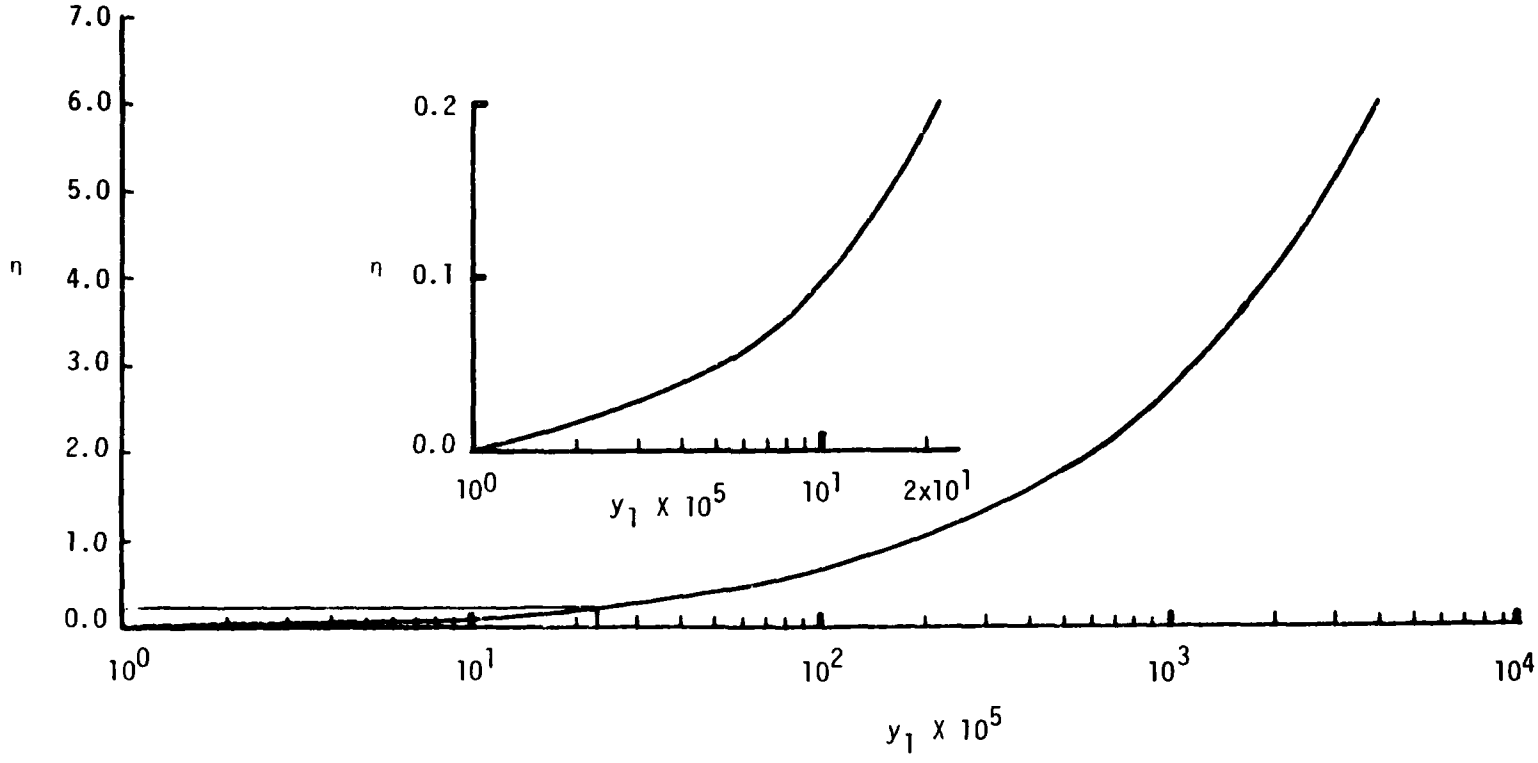

Figure 19. Relationship between η and y_1 at local Reynolds number $Re_x=1x10^6$ from case XI.

CHAPTER IX
CONCLUDING REMARKS

In this study the applicability as well as the accuracy and efficiency of a finite element-differential method has been investigated in detail for steady, two dimensional, incompressible turbulent boundary layer flow problems. The two-layer eddy viscosity closure model was utilized to simulate the Reynolds stress and provide a reasonable modeling of turbulent flows. The resulting system of partial differential equations has been transformed into the proper form for application of the finite element-differential method.

In the solution method, the transformed partial differential equation is first reduced into a system of first order nonlinear ordinary differential equations by a subdomain collocation method, in which the unknown function at a streamwise station is represented by a classical spline function. The reduced initial value problem was then integrated numerically by the modified Hamming's 4th order predictor-corrector method as well as by the Gear method for stiff equations.

A number of numerical experiments have been conducted on the boundary layer problem of flow over a flat plate which includes laminar, transitional, and turbulent flow regions. The numerical results show that the solution method can provide highly accurate results for the complete boundary layer flow field. In addition, the application of this method is simple and straightforward. For example, in Figure 14

the computed local skin-friction coefficient is in excellent agreement with the experimental data for the local Reynolds number up to 7.8×10^7.

The efficiency of numerical methods for boundary layer problems, in general, depends on how many nodal points are needed in the direction normal to the flow direction. Due to the better approximation of the solution profiles by the spline function and the transformations used to stretch the y coordinate, the number of nodal points required for the accurate solution in the present method has been significantly reduced as compared to previous methods. For example, for local Reynolds numbers less than 2×10^6, the present method needs only 8 nodal points to provide highly accurate results, while the higher order collocation method (Rubin and Khosla, 1977) and Keller's box scheme (Keller and Cebeci, 1972) may require 20 and 30 nodal points, respectively. Therefore the efficiency of the method of solution can be comparable to finite difference methods.

This study shows that when the local Reynolds number is sufficiently high, the solution profiles change too much near the wall. Consequently, due to this rapid changing of flow characteristics the choice of first element size is crucial to the accuracy of the solution. The valuable information about the variations of the first derivative w_1' at η_1, the second derivative w_0'' at η_0, and the displacement boundary layer thickness as a function of the local Reynolds number has been obtained. This information can give us a guide to properly choose the first element size. The results of numerical experiments show that a first element size of $h_1 = 0.1$ is small enough for the range of w_0'' less than 1.33; however, a much smaller value of $h_1 = 0.05$ is required for w_0'' between 1.33 and 9. For values of w_0'' greater than 9, it has been found

necessary to further cut down the first element size. For instance the values of $h_1 = 0.01$ and $h_1 = 0.05$ will be needed, respectively, for $24 \leq w_0'' \leq 32$ ($3.0 \times 10^7 \leq Re_x \leq 7.0 \times 10^7$) and $32 \leq w_0'' \leq 62$ ($7.0 \times 10^7 \leq Re_x \leq 5.0 \times 10^8$). For w_0'' greater than 62, it is expected that the first element size which is less than 0.005 should be used.

The results obtained in this study show that the finite element-differential method can be efficient and provide highly accurate results for the turbulent flow problems. Moreover, the computer program can be implemented to automatically select the value of the first element size based on the computed value of w_0'' and w_1'. It is expected that there will be little difficulty in extending the method of solution to flow past more complex geometries with the two-layer eddy viscosity model or with other transport-equation closure models.

APPENDIX A
EDDY VISCOSITY MODEL

Over the years, the eddy-viscosity model has been one of the most popular and extensively used models. Boussinesq [31] was the first to attack the problem of finding a model for the Reynolds stress $-\rho\overline{u'v'}$ by introducing the concept of eddy viscosity. He assumed that turbulent stresses act like viscous stresses, which implies that turbulent stresses are proportional to the mean velocity gradient. The coefficient of proportionality was called "eddy viscosity" and was defined by

$$\nu_t \equiv \frac{-\rho\overline{u'v'}}{\rho\frac{\partial u}{\partial y}} \tag{A-1}$$

When the model is applied to boundary layer flow problems, the boundary layer is regarded as a composite layer consisting of inner and outer regions, and the distributions of kinematic eddy viscosity are described by a separate empirical expression in each region.

The determination of eddy viscosity in the inner region depends on the Prandtl's mixing length theory. The distribution of the eddy viscosity in this region is given by (e.g. Schlichting, 1979)

$$(\nu_t)_i = \ell^2\left|\frac{\partial u}{\partial y}\right| \quad , \tag{A-2}$$

where ℓ is the mixing length and is proportional to y, that is,

$$\ell = ky \quad , \tag{A-3}$$

in which k is the so-called universal constant and its numerical value is to be determined from the experiment. For flows at high Reynolds number, k has a value of 0.4. However, in the viscous sublayer, which is very close to the wall, the mixing length theory is not valid. There have been numerous attempts to extend equation (A-3) to include the viscous sublayer by multiplying the mixing length by some functions. Van Driest [32] deduced from an analysis based upon experimental data and the second problem of Stokes [33] that the correct form for the mixing length in the inner layer including the viscous sublayer is

$$\ell = ky\,[1 - \exp(-\frac{y}{A})] \quad , \tag{A-4}$$

where the exponential term is due to the damping effect of the wall on the turbulent fluctuations and approaches zero at the outer edge of the viscous sublayer so that the law of the wall as expressed in equation (A-3) is valid.

The damping constant A in equation (A-4) is given by

$$A = A^{+}\,\nu/u_{\tau} \quad , \tag{A-5}$$

where A^{+} denotes an empirical constant equal to 26 for flat-plate flow (Van Driest, 1956) and u_{τ}, the friction velocity, was defined by

$$u_{\tau} \equiv (\tau_{w}(x)/\rho)^{\frac{1}{2}} \quad . \tag{A-6}$$

For incompressible flow with pressure gradient A^{+} is expected to vary somewhat with pressure gradient and was given by (Reynolds and Cebeci, [34]

$$A^{+} = 26(1 - \frac{\nu}{\rho u_{\tau}^{3}}\frac{dp}{dx})^{-\frac{1}{2}} . \tag{A-7}$$

Equations (A-4), (A-5) and (A-7) incorporated with equation (A-2) give the formulation of the kinematic eddy viscosity distribution in the inner region.

The formulation of the eddy viscosity in the outer region is based upon the Clauser [35] model. The eddy viscosity in the outer region is scaled by the displacement boundary layer thickness δ^* and the external velocity U(x). Therefore,

$$(\nu_t)_0 = k_2 U(x) \delta^* \quad . \tag{A-8}$$

The value of k_2 in equation (A-8) must be deduced from experiment and has a value of 0.0168 (Matsui, [36]). However, Mellor and Gibson [37] used 0.016 in their computation rather than 0.0168.

To improve the calculation of the shear-stress distribution across the boundary layer, equation (A-8) needs to be modified by a transverse intermittency factor γ; that is,

$$(\nu_t)_0 = k_2 \, U(x) \delta^* \gamma \quad , \tag{A-9}$$

in which γ was obtained by curve fit of measured data and given by (Reynolds and Cebeci, 1978)

$$\gamma = [1 + 5.5 \, (\frac{y}{\delta})^6]^{-1} \quad , \tag{A-10}$$

where δ is the boundary layer thickness.

Equations (A-2) and (A-9) may be multiplied by a transitional intermittency factor γ_t which accounts for the transitional region between the laminar and turbulent flow regions. According to Chen and Thyson [38], the transitional intermittency factor γ_t derived from

experimental data for incompressible flow is

$$\gamma_t = 1 - \exp\left[-\frac{U^3(x)}{1200\nu^2} R_{x_{tr}}^{-1.34} (x - x_{tr}) \int_{x_{tr}}^{x} \frac{ds}{u(s)}\right] , \quad \text{(A-11)}$$

where x_{tr} is the location of the start of transition and $R_{x_{tr}} \equiv \frac{U(x)x_{tr}}{\nu}$.

According to the eddy viscosity model, the two separate expressions for the distribution of kinematic eddy viscosity, including transverse and transitional intermittency factors become

$$(\nu_t)_i = \{ky\left[1 - \exp\left(-\frac{y}{A}\right)\right]^2\}\left|\frac{\partial u}{\partial y}\right|\gamma_t \quad \text{(A-12)}$$

$$(\nu_t)_0 = k_2 U(x)\delta^*\gamma\gamma_t . \quad \text{(A-13)}$$

Equations (A-12) and (A-13) can be used to describe the distribution of the kinematic eddy viscosity for boundary layer flow with and without a pressure gradient. The location of the matching point separating the inner and outer regions can be determined with the condition

$$(\nu_t)_i = (\nu_t)_0 . \quad \text{(A-14)}$$

The eddy viscosity model has been used with considerable success to compute a wide range of turbulent boundary layer flows. This model does not, however, allow for the transport of turbulent properties which do not appear parametrically in the equations of mean motion and its applicability is limited to near-equilibrium flows, which encompass most engineering problems.

REFERENCES

1. Reynolds, W. C., "Computation of Turbulent Flows", Annual Review of Fluid Mechanics, Vol. 8, 1976, pp. 183-208.

2. Mellor, G. L., and H. J. Herring, "Two Methods of Calculating Turbulent Boundary Layer Behavior Based on Numerical Solutions of the Equations of Motion I, Mean Velocity Field Method; II, Mean Turbulent Field Method, "Proceedings of the 1968 Conference on Turbulent Boundary Layer Prediction, Stanford University, 1968, pp. 331-345.

3. Cebeci, T., and A. M. O. Smith, "A Finite-Difference Solution of the Incompressible Turbulent Boundary-Layer Equations by an Eddy-Viscosity Concept", Proceedings of the 1968 Conference on Turbulent Boundary Layer Prediction, Stanford University, 1968, pp. 346-355.

4. Ng, K. H., S. V. Patankar, and D. B. Spalding, "The Hydrodynamic Turbulent Boundary Layer on a Smooth Wall, Calculated by a Finite-Difference Method, "Proceedings of the 1968 Conference on Turbulent Boundary Layer Prediction, Stanford University, 1968, pp. 356-365.

5. Cebeci, T., and A. M. O. Smith, Analysis of Turbulent Boundary Layer, Academic Press, New York, 1974.

6. Keller, H. B., and T. Cebeci, "Accurate Numerical Methods for Boundary Layer Flows - II. Two-Dimensional Turbulent Flows", AIAA Journal, Vol. 10, No. 9, 1972, pp. 1193-1199.

7. Blottner, F. G., "Variable Grid Scheme Applied to Turbulent Boundary Layer", Computer Methods in Applied Mechanics and Engineering, Vol. 4, 1974, pp. 179-194.

8. Rubin, S. G., and P. K. Khosla, "Turbulent Boundary Layers with and without Mass Injection", Computers and Fluids, Vol. 5, 1977, pp. 241-259.

9. Hsu, C. C., "The Use of Splines for the Solution of the Boundary-Layer Equations", Technical Report AFFDL-TR-75-158, Air Force Wright Aeronautical Laboratories, AFSC, WPAFB, 1976.

10. Hsu, C. C., and A. Liakopoulos, "A Finite Element-Differential Method for a Class of Compressible Laminar Boundary Layer Flows", The Second International Conference on Numerical Methods in Laminar and Turbulent Flow, 1981, pp. 497-504.

11. White, F. M., Viscous Flow, McGraw-Hill, New York, 1974, pp. 453-458.

12. Yih, C. S., Fluid Mechnics: A Concise Introduction to the Theory, corrected edition, West River Press, Ann Arbor, Michigan, 1977, pp. 422-423.

13. Guderley, K. G., and C. C. Hsu, "Numerical Integration of the Equations for the Steady Incompressible Boundary Layer", Technical Report ARL 72-0122, Aerospace Research Laboratories, United States Air Force, 1972.

14. Schlichting, H., Boundary-Layer Theory, McGraw-Hill, New York, 1979.

15. Greville, T. N. E., "Introduction to Spline Function", in Theory and Applications of Spline Functions, edited by T. N. E. Greville, Academic Press, New York, 1969, pp. 1-35.

16. Ahlberg. J. H., E. N. Nilson, and J. L. Walsh, The Theory of Splines and Their Application, Academic Press, New York, 1967.

17. De Boor, C., "On Calculating with B-Splines", Journal of Approximation Theory 6, 1972, pp. 50-62.

18. Panton, R. L., and H. B. Sallee, "Spline Function Representations for Computer Solution to Fluid Problems", Computers and Fluids, Vol. 3, 1975, pp. 257-269.

19. Rubin, S. G., and P. K. Khosla, "Higher Order Numerical Solutions Using Cubic Splines", AIAA Journal, Vol. 14, No. 7, 1976, pp. 851-858.

20. Inoue, M., M. Kuroumaru, and S. Yamaguchi, "A Solution of Fredholm Integral Equation by Means of the Spline Fit Approximation", Computers and Fluids, Vol. 7, 1979, pp. 33-46.

21. Hildebrand, F. B., Introduction to Numerical Analysis, McGraw-Hill, New York, 1974, pp. 478-494.

22. Hornbeck, R. W., Numerical Method, Quantum Publishers, New York, 1975, pp. 85-101.

23. Krylov, V. I., Approximate Calculation of Integrals, Macmillan, New York, 1962.

24. Ralston, A., "Numerical Integration Methods for the Solution of Ordinary Differential Equations", in Mathematical Methods for Digital Computers, edited by H. S. Wilf, iley, New York, 1960, pp. 85-109.

25. Gear, C. W., Numerical Initial Value Problems in Ordinary Differential Equations, Pretice-Hall, Englewood Cliffs, New Jersey, 1971b.

26. Hindmarsh, A. C., "GEAR: Ordinary Equation System Solver", Lawrence Livermore Laboratory, Report UCID-30001, Revision 3, 1974.

27. Dhawan, S., "Direct Measurements of Skin Friction", NACA Technical Note No. 2567, 1952.

28. Smith, D. W., and J. H. Walker, "Skin Friction Measurements in Incompressible Flow", NASA Technical Report R-26, 1959.

29. Winter, K. G., and L. Gaudet, "Turbulent Boundary-Layer Studies at High Reynolds Numbers at Mach Number Between 0.2 and 2.8", RAE Technical Report 70251, 1970.

30. Gear, C. W., "DIFSUB for Solution of Ordinary Differential Equations", Communications of the ACM, Vol. 14, No. 3, 1971a, pp. 185-190.

31. Boussinesq, J., "Theorie de l'ecoulement Tourbillant", Mem. Pres. Acad. Sci., Vol. 23, Nov 46, Paris, 1977.

32. Van Driest, E. R., "On Turbulent Flow Near a Wall", Journal Aeronautical Science, Vol. 23, No. 11, 1956, pp. 1007-1011.

33. Stokes, G. G., "On the Effect of the Internal Friction of Fluids on the Motion of Pendulums", Mathematics and Physics Papers, Vol. 3, Cambridge, 1901, pp. 1-141.

34. Reynolds, W. C., and T. Cebeci, "Calculation of Turbulent Flows", Topics in Applied Physics, Turbulence, Vol. 12, edited by P. Bradshaw, 1978, pp. 193-229.

35. Clauser, F. H., "The Turbulent Boundary Layer", Advances in Applied Mechanics, Vol. 4, 1956, pp. 1-51.

36. Matsui, T., "Mean Velocity Distribution in the Outer Layer of a Turbulent Boundary Layer", Research Report 42, Aerophysics Department, Mississippi State University, 1963.

37. Mellor, G. L., and D. M. Gibson, "Equilibrium Turbulent Boundary Layers", Journal of Fluid Mechanics, Vol. 24, 1966, pp. 225-253.

38. Chen, K. K., and N. A. Thyson, "Extension of Emmon's Spot Theory to Flows on Blunt Bodies". AIAA Journal, Vol. 9, No. 5, May 1974, pp. 821-825.

☆U.S.Government Printing Office: 1982 — 559-005/4054

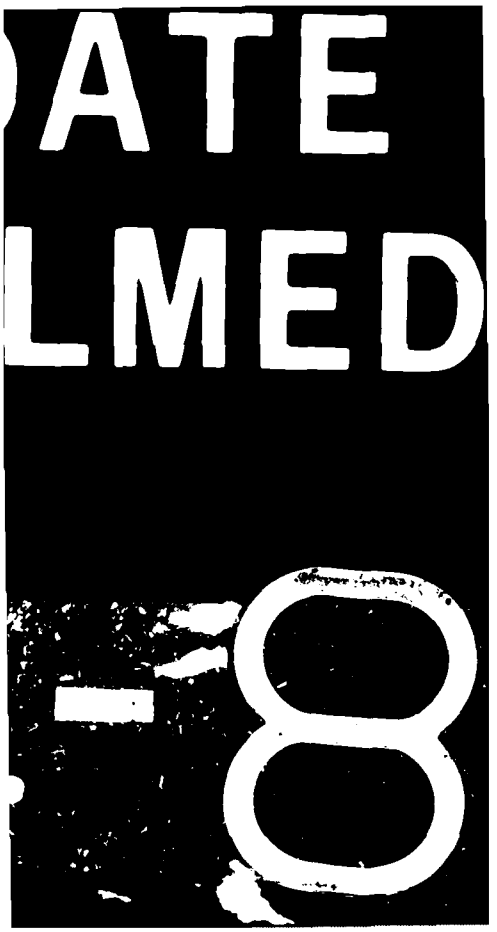
ATE
LMED
8